NASA TECHNICAL MEMORANDUM

NASA TM X-3316

NASA TM X-3316

AN INVESTIGATION OF FRACTURE TOUGHNESS, FATIGUE-CRACK GROWTH, SUSTAINED-LOAD FLAW GROWTH, AND IMPACT PROPERTIES OF THREE PRESSURE VESSEL STEELS

C. Michael Hudson, J. C. Newman, Jr., and Peter E. Lewis

Langley Research Center
Hampton, Va. 23665

NATIONAL AERONAUTICS AND SPACE ADMINISTRATION • WASHINGTON, D. C. • DECEMBER 1975

1. Report No. NASA TM X-3316	2. Government Accession No.	3. Recipient's Catalog No.
4. Title and Subtitle AN INVESTIGATION OF FRACTURE TOUGHNESS, FATIGUE-CRACK GROWTH, SUSTAINED-LOAD FLAW GROWTH, AND IMPACT PROPERTIES OF THREE PRESSURE VESSEL STEELS		5. Report Date December 1975
		6. Performing Organization Code
7. Author(s) C. Michael Hudson, J. C. Newman, Jr., and Peter E. Lewis		8. Performing Organization Report No. L-10447
9. Performing Organization Name and Address NASA Langley Research Center Hampton, Va. 23665		10. Work Unit No. 505-02-31-01
		11. Contract or Grant No.
12. Sponsoring Agency Name and Address National Aeronautics and Space Administration Washington, D.C. 20546		13. Type of Report and Period Covered Technical Memorandum
		14. Sponsoring Agency Code
15. Supplementary Notes		

16. Abstract

Tests to determine fracture toughness, fatigue-crack growth, sustained-load flaw growth, and impact properties were conducted on three pressure vessel steels: A. O. Smith VMS 5002 and VMS 1146A, and ASTM A-225 Gr.B. The data obtained will help relieve the general paucity of such data on these pressure vessel steels.

The elastic fracture toughness of the three steels does not decrease significantly with decreasing temperature from room temperature to about 244 K (-20° F). The elastic fracture toughness of the three steels increases with increasing specimen width and thickness.

The fatigue-crack-growth data for all three steels fall into relatively narrow scatter bands on plots of rate against stress-intensity range. Barsom's equation (Transactions ASME, Journal of Engineering for Industry, Nov. 1971) predicts the upper bounds of the scatter bands reasonably well.

Charpy impact energies decrease with decreasing temperature in the nominal temperature range from room temperature to 244 K (-20° F).

The nil-ductility temperatures of VMS 5002 and A-225 Gr.B are 250 K (-10° F) and 241 K (-25° F), respectively. A lack of test material precluded obtaining the nil-ductility temperature of VMS 1146A.

17. Key Words (Suggested by Author(s))		18. Distribution Statement	
VMS 5002 VMS 1146A A-225 Gr.B Fracture toughness Fatigue-crack growth		Unclassified – Unlimited Subject Category 26	
19. Security Classif. (of this report) Unclassified	20. Security Classif. (of this page) Unclassified	21. No. of Pages 54	22. Price* $4.25

*For sale by the National Technical Information Service, Springfield, Virginia 22161

AN INVESTIGATION OF FRACTURE TOUGHNESS, FATIGUE-CRACK GROWTH, SUSTAINED-LOAD FLAW GROWTH, AND IMPACT PROPERTIES OF THREE PRESSURE VESSEL STEELS

C. Michael Hudson, J. C. Newman, Jr.,
and Peter E. Lewis
Langley Research Center

SUMMARY

Tests to determine fracture toughness, fatigue-crack growth, sustained-load flaw growth, and impact properties were conducted on three pressure vessel steels: A. O. Smith VMS 5002 and VMS 1146A, and ASTM A-225 Gr.B. The data obtained will help relieve the general paucity of such data on these pressure vessel steels.

The elastic fracture toughness of the three steels does not decrease significantly with decreasing temperature from room temperature to about 244 K (-20° F). The elastic fracture toughness of the three steels increases with increasing specimen width and thickness.

The fatigue-crack-growth data for all three steels fall into relatively narrow scatter bands on plots of rate against stress-intensity range. Barsom's equation (Transactions ASME, Journal of Engineering for Industry, Nov. 1971) predicts the upper bounds of the scatter bands reasonably well.

Charpy impact energies decrease with decreasing temperature in the nominal temperature range from room temperature to 244 K (-20° F).

The nil-ductility temperatures of VMS 5002 and A-225 Gr.B are 250 K (-10° F) and 241 K (-25° F), respectively. A lack of test material precluded obtaining the nil-ductility temperature of VMS 1146A.

INTRODUCTION

The development of fracture mechanics analysis into a practical tool for predicting the behavior of cracked structures has precipitated a need for fracture toughness and fatigue-crack-growth data on many materials. Relatively large quantities of such data have been generated for materials used for aerospace applications (ref. 1). However, there are relatively few such data on materials used for pressure vessel applications. Consequently, when a fracture mechanics analysis was recently performed on a series of pressure vessels at the Langley Research Center, the needed data had to be generated. A series of fracture-toughness and fatigue-crack-growth tests were conducted on three pressure vessel steels: A. O. Smith VMS 5002, A. O. Smith VMS 1146A, and ASTM A-225 Gr.B. The test temperatures ranged from room temperature to 227 K (-50° F) in the fracture-toughness tests. The test temperature was room temperature in the fatigue-crack-growth tests.

Sustained-load flaw-growth, Charpy impact fracture, and drop-weight impact fracture experiments were conducted on the three steels. Properties determined by these experiments were also needed in evaluating the integrity of the vessels.

This report presents the results of all experiments conducted. The results can be used to predict crack growth and failure in these three pressure vessel steels. The Charpy results are suitable for determining the minimum allowable operating temperature for the steels, according to the current ASME Boiler and Pressure Vessel Code (ref. 2).

Chicago Bridge & Iron Company and Lenape Forge Division of Gulf & Western Industrial Products Company supplied the steels tested. Under contract to Langley Research Center (LaRC), the following companies performed the tests indicated: Spectrochemical Laboratories Inc., the chemical analysis; Martin Marietta Aerospace (jointly with LaRC), the fracture-toughness, fatigue-crack-growth, and sustained-load flaw-growth tests; Martin Marietta Aerospace, the Charpy impact tests; and Pittsburgh Testing Laboratory, the drop-weight tests.

SYMBOLS AND ABBREVIATIONS

Except for the figures, this paper presents physical quantities in both the International System of Units (SI) and the U.S. Customary Units. For clarity, the figures show only SI units. All measurements and calculations were made in U.S. Customary Units. Reference 3 presents factors relating the two systems, and appendix A presents those factors used in the present investigation.

a crack length, mm (in.)

a_i crack length at start of fracture-toughness test, mm (in.)

a_{sl} crack length at start of sustained-load flaw-growth test, mm (in.)

C_{VN} energy absorbed in impact test on Charpy V-notch specimen, N-m (ft-lbf)

da/dN rate of fatigue-crack growth, nm/cycle (in/cycle)

e	elongation in 51-mm (2-in.) gage length, percent
$\dot{K}$	rate of change of stress intensity factor with time, $(MN/m^{3/2})/s$ $(ksi\text{-}in^{1/2}/min)$
ΔK	stress-intensity-factor range, $MN/m^{3/2}$ $(ksi\text{-}in^{1/2})$
K_F	material fracture-toughness parameter, $MN/m^{3/2}$ $(ksi\text{-}in^{1/2})$
K_{Ie}	elastic fracture toughness, $MN/m^{3/2}$ $(ksi\text{-}in^{1/2})$
K_{Ii}	elastic stress-intensity factor at start of sustained-load flaw-growth test, $MN/m^{3/2}$ $(ksi\text{-}in^{1/2})$
K_{max}	maximum stress-intensity factor, $MN/m^{3/2}$ $(ksi\text{-}in^{1/2})$
K_{min}	minimum stress-intensity factor, $MN/m^{3/2}$ $(ksi\text{-}in^{1/2})$
l_e	lateral expansion obtained from Charpy impact test, mm (in.)
m	material fracture-toughness parameter
P_f	maximum load applied to specimen during fracture-toughness test, N (lbf)
P_{max}	maximum applied load, N (lbf)
P_{min}	minimum applied load, N (lbf)
R	ratio of minimum stress to maximum stress
S_n	elastic nominal failure stress, Pa (ksi)
S_u	elastic nominal stress required to produce fully plastic hinge on net section, Pa (ksi)
T	test temperature, K (^oF)
t	specimen thickness, mm (in.)

w	specimen width, mm (in.)
σ_u	ultimate tensile strength, Pa (ksi)
σ_y	yield strength (0.2-percent offset), Pa (ksi)

Abbreviations:

COD	crack opening displacement
CS	compact specimen configuration
LVDT	linear variable differential transformer
NDT	nil-ductility temperature, K (^oF)
NFG	no flaw growth in sustained-load flaw-growth test
WOL	wedge-opening-load specimen configuration

SPECIMENS, TESTS, AND PROCEDURES

Specimens

Test specimens were made of VMS 5002, VMS 1146A, and A-225 Gr.B ferritic steels. The VMS 5002 and VMS 1146A are proprietary steels developed by A. O. Smith Corporation for fabricating laminated pressure vessels. The A-225 Gr.B is an ASTM pressure vessel steel (ref. 4). Table I presents the results of the tensile and chemical tests conducted on the three steels tested in this investigation. The specimens used to obtain the tensile properties met ASTM standards (ref. 5).

As mentioned in the Introduction, several laboratories generated the data presented herein. Each laboratory used specimen configurations adaptable to the testing equipment on hand. Consequently, two, and sometimes three, specimen configurations were tested to determine fracture toughness, fatigue-crack growth, and sustained-load flaw growth. The results of these tests were analyzed by using the appropriate stress-intensity factor for each configuration.

Fracture-toughness specimens.- Figures 1, 2, and 3 show the configurations of the compact specimens (CS) tested. The following table gives the configurations, thicknesses, and widths of the various specimens for each material:

Material	Configuration		Specimen thickness		Specimen width	
	Type	Figure	mm	in.	mm	in.
VMS 5002	CS	1(a)	25.4	1.0	50.8	2.0
	CS	1(b)	45.7	1.8	91.4	3.6
	CS	1(c)	109.2	4.3	71.1	2.8
VMS 1146A	CS	1(a)	25.4	1.0	50.8	2.0
	CS	2	25.4	1.0	91.4	3.6
A-225 Gr.B	CS	1(a)	25.4	1.0	50.8	2.0
	CS	1(b)	45.7	1.8	91.4	3.6
	CS	3	83.8	3.3	71.1	2.8

A chevron notch was machined into each specimen to initiate fatigue cracks. The 25.4- and 45.7-mm (1.0- and 1.8-in.) thick specimens met at the ASTM standards (ref. 6) for specimen configuration. The 83.8- and 109.2-mm (3.3- and 4.3-in.) thick specimens did not meet the ASTM standards; however, a boundary collocation analysis (ref. 7) gave stress-intensity factors for these nonstandard specimens. These factors were used to calculate the fracture toughness of the specimens at failure.

Fatigue-crack-growth specimens.- Figures 1(a) and 4 show the configurations of the compact specimens (CS) tested. The following table gives the thicknesses and widths of the specimens:

Material	Configuration		Specimen thickness		Specimen width	
	Type	Figure	mm	in.	mm	in.
All three steels	CS	1(a)	25.4	1.0	50.8	2.0
All three steels	CS	4	5.1	0.2	63.5	2.5

Chevron and straight-through notches were machined into the 25.4-mm (1.0-in.) thick and the 5.1-mm (0.2-in.) thick specimens, respectively, to initiate fatigue cracks. Fine lines scribed on the surfaces of the 25.4-mm (1.0-in.) thick specimens marked intervals along the crack path. The spacing between lines was 1.3 mm (0.050 in.). These scribe lines provided a means of monitoring crack growth but, being parallel to the loading direction, introduced no stress concentration in the specimens. The 5.1-mm (0.2-in.) thick specimens required no scribe lines, because a crack-opening-displacement (COD) gage monitored crack growth.

Sustained-load flaw-growth specimen.- Figures 1(a) and 5 show the configurations of the compact (CS) and wedge-opening-load (WOL) specimens tested. The following table gives the thicknesses and widths of the specimens:

Material	Configuration		Specimen thickness		Specimen width	
	Type	Figure	mm	in.	mm	in.
All three steels	CS	1(a)	25.4	1.0	50.8	2.0
VMS 5002 and A-225 Gr.B	WOL	5(a)	35.6	1.4	91.4	3.6
VMS 1146A	WOL	5(b)	25.4	1.0	91.4	3.6

Chevron and straight-through notches were machined into the CS and WOL specimens, respectively, to initiate fatigue cracks.

Charpy impact specimens.- Figure 6 shows the configuration of the Charpy impact specimens tested. These specimens were 55.9 mm (2.2 in.) long and 10.2 mm (0.4 in.) thick. A 2.0-mm (0.08-in.) deep V-notch was cut into the center of each specimen to initiate failure. This configuration met the ASTM standards (ref. 8) for Charpy impact specimens. Specimens were machined from all three steels.

Drop-weight test specimens.- Figure 7 shows the configuration of the drop-weight specimens tested. These specimens were 127.0 mm (5.0 in.) long, 50.8 mm (2.0 in.) wide, and 15.7 mm (0.62 in.) thick. A brittle weld bead was laid in the center of each specimen, and a notch cut across the crown of the weld to initiate failure. This configuration met the ASTM standards (ref. 9) for drop-weight specimens. Specimens were machined from VMS 5002 and A-225 Gr.B steels only. A lack of material precluded drop-weight testing the VMS 1146A.

Testing Machines

Fracture-toughness testing machines.- The following table lists the capabilities of the three testing machines used for the fracture-toughness tests:

Machine type	Maximum load capacity		Machine description source
	kN	lbf	
Hydraulic	89	20 000	Ref. 10
Hydraulic	445	100 000	Appendix B
Hydraulic	4448	1 000 000	Appendix B

Fatigue-crack-growth testing machines.- The following table lists the capabilities of the two testing machines used for the fatigue-crack-growth tests:

Machine type	Maximum load capacity		Operating frequency used		Machine description source
	kN	lbf	Hz	cpm	
Inertia force compensation	89	20 000	20	1200	Ref. 11
Hydraulic	445	100 000	5 to 10	300 to 600	Appendix B

Sustained-load flaw-growth testing machine.- Static loads were applied to the CS specimens by a tester having a 44-kN (10 000-lbf) static load capacity (ref. 12). Static loads were applied to the WOL specimens by tightening the bolt which is threaded through the upper half of the specimen and butts against the lower half. (See fig. 5.)

Charpy impact and drop-weight testers.- Standard Charpy impact and drop-weight testers were used for the impact and drop-weight tests. References 8 and 9 describe the test apparatus in detail.

Test Procedures

Fracture-toughness tests.- Test specimens were fatigue cracked to predetermined lengths (final a/w values varied from 0.375 to 0.625) by applying constant-amplitude fatigue loadings with $R \approx 0$ and $\Delta K \leqq 0.30K_{Ie}$. This cracking was done at room temperature. The specimens were then cooled (if called for in the test program) and monotonically loaded to failure at stress-intensity rates $\dot{K}$ between 0.92 and 2.75 $\left(MN/m^{3/2}\right)/s$ $\left(50 \text{ and } 150 \text{ ksi-in}^{1/2}/\text{min}\right)$. Throughout each fracture-toughness test a calibrated COD gage was mounted in the machined notch of each specimen. The output from this gage and the output from the testing-machine load cell were continuously recorded for each specimen. These records indicated the maximum load at failure.

The 71.1-mm (2.8-in.) wide VMS 5002 and A-225 Gr.B specimens were cooled to the test temperature by flowing cold nitrogen gas into a plastic shroud taped around the test section. Once the test temperature was reached, the flow of cool gas was manually controlled to keep the specimen at the test temperature. The specimens were held at the test temperature for 3.6 ks (1 hr), and then were pulled to failure. A thermocouple spot-welded to the specimen was used to record specimen temperature.

The 91.4-mm (3.6-in.) wide VMS 5002, VMS 1146A, and A-225 Gr.B specimens were cooled to the test temperature by pouring a mixture of alcohol and dry ice into a container surrounding the test section. Dry ice was added to the mixture until the specimen temperature approached the test temperature. Once the test temperature was reached, small quantities of dry ice were added to the mixture in order to keep the solution at the test temperature. The specimens were held at the test temperature for approximately 1.8 ks (1/2 hr), and then were pulled to failure. A thermocouple spotwelded to the specimen indicated specimen temperature.

The 50.8-mm (2.0-in.) wide VMS 5002, VMS 1146A, and A-225 Gr.B specimens were all tested at room temperature.

Fatigue-crack-growth tests.- Constant-amplitude loadings were applied in most tests. However, in several tests, specimens were tested at two stress amplitudes. The stress-intensity ranges ΔK applied in the crack-growth tests varied from 20 to 73 $MN/m^{3/2}$ (18 to 66 ksi-in$^{1/2}$). The stress ratio used was approximately zero (R = 0.05), and the test temperature was room temperature.

Fatigue-crack growth in the 50.8-mm (2.0-in.) wide specimens was visually monitored. The number of cycles required to propagate the cracks to each scribe line was recorded. The crack growth rates were calculated from the slope of the plots of crack length against number of cycles.

A calibrated COD gage mounted in the machined notch was used to monitor fatigue-crack growth in the 63.5-mm (2.5-in.) wide specimens. The load-displacement data were recorded against the number of cycles. Analysis of these records gave crack growth rates in these specimens.

Sustained-load flaw-growth tests.- Constant-amplitude fatigue loadings with $R \approx 0$ and $\Delta K \leqq 0.5K_{Ie}$ were applied to the test specimens until fatigue cracks of predetermined length were developed. (Final a/w values varied from 0.48 to 0.55.) Sustained-load flaw-growth tests at room temperature were then conducted in air, in distilled water, and in distilled water containing a rust inhibitor. The K_{Ie} values applied in these tests ranged from 107 to 67 $MN/m^{3/2}$ (97 to 61 ksi-in$^{1/2}$), and the maximum testing time was greater than 3600 ks (1000 hr).

Different test procedures were used to load and wet the different width specimens. For the 50.8-mm (2.0-in.) wide specimens, load was applied by manually tightening the mean-load spring on the testing machine (ref. 12) until the desired load was reached. (A calibrated, load-readout system on the testing machine indicated the load.) However, the compliance of the specimens tended to increase with crack growth and caused a relaxation in the load. Consequently, the load was periodically adjusted in order to keep the load approximately constant. During tests in aqueous environments, the 50.8-mm (2.0-in.) wide specimens were immersed by flowing the desired liquid into a plastic shroud taped around the test section.

For the 91.4-mm (3.6-in.) wide specimens, load was applied by manually tightening the loading bolts (fig. 5) until the desired load was reached. (A calibrated COD gage mounted in the machined notch was used as a load indicator.) No crack growth occurred in these tests; consequently, there was no need to adjust loadings during the tests. During tests in aqueous environments, the entire 91.4-mm (3.6-in.) wide specimen was submerged in a bath filled with the desired liquid.

Charpy impact and drop-weight tests.- The Charpy impact and drop-weight specimens were tested in accordance with the procedures specified in references 8 and 9, respectively.

RESULTS AND DISCUSSION

Fracture-Toughness Experiments

Table II presents the results of the fracture-toughness experiments on all three steels. This table gives the specimen thickness t, the specimen width w, the test temperature T, the crack length at the start of the fracture-toughness test a_i, the maximum load applied to the specimen during the fracture-toughness test P_f, and the elastic fracture toughness K_{Ie}. Equations (C1) to (C4) in appendix C were used to calculate the K_{Ie} values. Figures 8, 9, and 10 show the variation of K_{Ie} with temperature for the VMS 5002, VMS 1146A, and A-225 Gr.B specimens, respectively. These figures indicate that, for all three steels, K_{Ie} does not decrease significantly with decreasing temperature from room temperature to about 244 K (-20° F). However, the larger specimen thicknesses and specimen widths tended to produce larger K_{Ie} values for the three steels.

Newman's elastic-plastic failure analysis (refs. 13 and 14) was also used to analyze the fracture-toughness data. Equation (C5), appendix C, is the pertinent relationship for this analysis. The material fracture-toughness parameters K_F and m in equation (C5) were determined with a best-fit procedure described in reference 13. Figures 11, 12, and 13 show the variation of K_{Ie} with specimen width for the 25.4- and 45.7-mm (1.0- and 1.8-in.) thick specimens. These figures show that K_{Ie} is larger for larger specimen widths, as predicted by Newman's analysis (solid curve). Figures 11 to 13 do not include the data for the 83.8- and 109.2-mm (3.3- and 4.3-in.) thick specimens. These data are excluded because, as appendix C explains, K_F and m vary with thickness. Consequently, the values of K_F and m shown in these figures do not apply for the thicker specimens. The thickness difference between the 25.4- and 45.7-mm (1.0- and 1.8-in.) thick specimens is considered insignificant as far as K_F and m are concerned.

Figure 14 shows the variation of K_{Ie} with a/w for the 25.4-mm (1.0-in.) thick VMS 5002 specimens. The larger values of a/w produce smaller K_{Ie} values. Newman's analysis accounted for this trend.

Fatigue-Crack-Growth Experiments

Table III presents the results of the fatigue-crack-growth experiments on all three steels. This table gives the stress-intensity-factor range ΔK and the corresponding fatigue-crack-growth rate da/dN. The stress-intensity-factor range was calculated from equations (C7) to (C9) in appendix C.

Figures 15, 16, and 17 show the variations of da/dN with ΔK for the steels VMS 5002, VMS 1146A, and A-225 Gr.B, respectively. The data from the different laboratories fell into relatively narrow scatter bands. These figures also show a plot of Barsom's equation (ref. 15). This equation has the form

$$\frac{da}{dN} = \left(6.92 \times 10^{-3}\right)(\Delta K)^3 \tag{1}$$

where the coefficient 6.92×10^{-3} is for SI Units. (The coefficient for U.S. Customary Units is 3.6×10^{-10}.) Barsom showed that this equation fit the upper boundary of the da/dN data generated in tests on a large number of ferrite-pearlite steels. This equation fits the upper boundary of the VMS 5002 and A-225 Gr.B data very well (figs. 15 and 17). The equation fell somewhat below the upper boundary of the VMS 1146A data (fig. 16). However, this underestimation was not large. Thus, the present data further verify Barsom's equation as a useful tool for predicting an upper boundary on crack growth rates in ferrite-pearlite steels.

Sustained-Load Flaw-Growth Experiments

Table IV presents the results of the sustained-load flaw-growth experiments on the three steels. This table gives the test fluid, specimen width w, crack length at the start of the sustained-load flaw-growth test a_{sl}, the maximum load applied to the specimen P_{max}, the stress-intensity factor applied at the start of the tests K_{Ii}, the test duration, and whether failure occurred or not. The stress-intensity factors were calculated from equations (C8) and (C10) in appendix C.

Figures 18, 19, and 20 show a plot of K_{Ii} against test duration. Arrows on the symbols indicate test specimens which did not fail. No failures occurred in either VMS 5002 or VMS 1146A. The highest K_{Ii} value applied for these two materials was 107 $MN/m^{3/2}$ (97 ksi-$in^{1/2}$) for VMS 5002 and 79 $MN/m^{3/2}$ (72 ksi-$in^{1/2}$) for VMS 1146A. Failures did occur in A-225 Gr.B, but only at K_{Ii} values greater than 78 $MN/m^{3/2}$ (71 ksi-$in^{1/2}$). Figures 18, 19, and 20 also indicate that distilled water had no adverse effect on sustained-load flaw growth.

Charpy Impact Experiments

Table V presents the results of the Charpy impact experiments on all three steels. This table gives the test temperature T, the energy absorbed during each test C_{VN}, and the lateral expansion on the compression side of each specimen l_e.

Figures 21, 22, and 23 show the variation of C_{VN} with temperature. For all three steels, C_{VN} values were smaller at lower temperatures in the nominal temperature range from room temperature to 244 K (-20° F).

The difference in the temperature effect for the fracture-toughness experiments $\left(K_{Ie} \approx \text{Constant}\right)$ and the Charpy impact experiments $\left(C_{VN}\right.$ proportional to temperature$\left.\right)$ over the same temperature range is probably due to the difference in loading rates for the two types of experiments. If the loading rates are sufficiently low, significant plastic deformation can occur at a crack or notch root before a specimen fails. In the fracture-toughness experiments with relatively low loading rates, this plastic deformation apparently enabled the steels to maintain their room temperature toughness at lower temperatures. In the Charpy impact experiments with very high loading rates, there was apparently insufficient time for significant plastic deformation, and, consequently, notch sensitivity increased with decreasing temperature.

Drop-Weight Experiments

Table VI presents the results of the drop-weight tests on VMS 5002 and A-225 Gr.B steels. This table gives the test temperature T, whether the test specimens broke or not, and the nil-ductility temperatures for the two steels. The nil-ductility temperature is the maximum temperature at which a standard drop-weight specimen breaks when tested according to prescribed methods (ref. 9). Table VI indicates that the nil-ductility temperatures of VMS 5002 and A-225 Gr.B are 250 K (-10° F) and 241 K (-25° F), respectively. A lack of material precluded drop-weight testing the VMS 1146A.

SUMMARY OF RESULTS

Tests to determine fracture toughness, fatigue-crack growth, sustained-load flaw growth, and impact properties were conducted on three pressure vessel steels: A. O. Smith VMS 5002 and VMS 1146A, and ASTM A-225 Gr.B. The results of these tests are summarized as follows:

1. The elastic fracture toughness of the three steels does not decrease significantly with decreasing temperature from room temperature to about 244 K (-20° F).

2. The elastic fracture toughness of the three steels increases with increasing specimen width. Newman's elastic-plastic failure analysis (Engineering Fracture Mechanics, Sept. 1973) accurately predicts this increase.

3. For all three steels, the data for fatigue-crack-growth rate fall into relatively narrow scatter bands on plots of rate against stress-intensity-factor range.

4. Barsom's equation (Transactions ASME, Journal of Engineering for Industry, Nov. 1971) predicts the upper boundary of the VMS 5002 and A-225 Gr.B fatigue-crack growth-rate data very well. However, the equation slightly underestimated the upper boundary of the VMS 1146A data.

5. The VMS 5002 and VMS 1146A specimens did not fail at stress-intensity factors of 107 and 79 $MN/m^{3/2}$ $(97$ and 72 ksi-in$^{1/2})$, respectively, in sustained-load flaw-growth tests. Some A-225 Gr.B specimens did fail at a stress-intensity factor of 79 $MN/m^{3/2}$ $(72$ ksi-in$^{1/2})$.

6. For all three steels, Charpy impact energies are smaller at lower temperatures, in the nominal temperature range from room temperature to 244 K (-20° F).

7. In standard drop-weight tests, VMS 5002 and A-225 Gr.B exhibit nil-ductility temperatures of 250 K (-10° F) and 241 K (-25° F), respectively.

Langley Research Center
National Aeronautics and Space Administration
Hampton, Va. 23665
November 17, 1975

APPENDIX A

CONVERSION OF SI UNITS TO U.S. CUSTOMARY UNITS

The International System of Units (SI) was adopted by the Eleventh General Conference on Weights and Measures held in Paris in 1960 (ref. 3). Conversion factors required for units used herein are given in the following table:

Physical quantity	SI Unit (a)	Conversion factor (b)	U.S. Customary Unit
Force	newtons (N)	0.2248	lbf
Length	meters (m)	0.3937×10^{2}	in.
Stress	pascals (Pa)	0.145×10^{-6}	ksi = 10^3 lbf/in^2
Stress intensity	newtons per meter$^{3/2}$ (N/m$^{3/2}$)	0.9099×10^{-6}	ksi-in$^{1/2}$
Frequency	hertz (Hz)	60	cpm
Temperature	kelvins (K)	$\frac{9}{5}$K - 459.7	^{o}F

[a] Prefixes and symbols to indicate multiples of units are as follows:

Multiple	Prefix	Symbol
10^{-9}	nano	n
10^{-6}	micro	μ
10^{-3}	milli	m
10^{3}	kilo	k
10^{6}	mega	M
10^{9}	giga	G

[b] Multiply value given in SI Unit by conversion factor to obtain equivalent in U.S. Customary Unit, or apply the conversion formula.

APPENDIX B

DESCRIPTION OF THE 445- AND 4448-kN (100 000- AND 1 000 000-lbf) TESTING MACHINES

The 445- and 4448-kN (100 000- and 1 000 000-lbf) testing machines are analog closed-loop servocontrolled hydraulic testing systems. (Fig. 24 shows a schematic diagram of these testing systems.) These systems may be used for either fracture-toughness or fatigue testing.

To use these systems for fracture-toughness testing, the operator sets the function generator to the ramp position and to the desired loading rate. The operator then initiates loading by pushing the load button on the function generator. The loading increases monotonically until the specimen fractures.

To use the systems for fatigue testing, the operator first applies the desired mean load by adjusting the mean-load potentiometer. He then (a) sets the function generator to the desired waveform (e.g., sine, square, or sawtooth) and to the desired loading frequency, and (b) sets the alternating-load potentiometer to the desired alternating load level. The operator initiates loading by pushing the run button on the function generator. The loading cycles about the mean load symmetrically until either the specimen fails or the loading is stopped.

In operation, the conditioned-command signal is fed into the servoloop summing point. The voltage from either the load cell transducer or the LVDT transducer is also fed into this summing point. The command and transducer voltages are summed, and suitably amplified, to form a signal which drives the servovalve. This servovalve directs oil to the appropriate side of the hydraulic cylinder to obtain the commanded load.

During fracture-toughness tests, loads are monitored and recorded on a calibrated oscillograph in order to determine the load at failure.

During fatigue tests, loads are monitored by comparing, on an oscilloscope, the output voltage from the load cell (or LVDT) with an adjustable bias voltage which corresponds to the desired load level for the test. When the sum of these voltages is zero, the desired load is on the test specimen. This comparison is made at both the maximum and the minimum loads in the cycle.

APPENDIX C

METHODS OF ANALYSES

Fracture Toughness

The fracture-toughness data were analyzed using both linear-elastic fracture mechanics (ref. 16) and an elastic-plastic failure analysis (refs. 13 and 14). The following relationships were used for the linear-elastic fracture mechanics analysis. For the 50.8- and 91.4-mm (2.0- and 3.6-in.) wide specimens, the elastic fracture toughness (elastic stress-intensity factor at failure) is given by

$$K_{Ie} = \left(\frac{P_f}{tw^{1/2}}\right) f_1\left(\frac{a}{w}\right) \tag{C1}$$

where from reference 7 (in the present notation)

$$f_1\left(\frac{a}{w}\right) = 4.55 - 40.32\left(\frac{a}{w}\right) + 414.7\left(\frac{a}{w}\right)^2 - 1698\left(\frac{a}{w}\right)^3 + 3781\left(\frac{a}{w}\right)^4 - 4287\left(\frac{a}{w}\right)^5 + 2017\left(\frac{a}{w}\right)^6 \tag{C2}$$

for a/w values from 0.2 to 0.8.

For the 71.1-mm (2.8-in.) wide specimens, the elastic fracture toughness is given by

$$K_{Ie} = \left(\frac{P_f}{tw^{1/2}}\right) f_2\left(\frac{a}{w}\right) \tag{C3}$$

Boundary-collocation analysis (ref. 7) indicates that for the a/w ratio of 0.55 used in this investigation,

$$f_2\left(\frac{a}{w}\right) = 12.59 \tag{C4}$$

Subsequent finite-element stress analysis confirmed the boundary-collocation results.

In equations (C1) to (C4), P_f is the maximum load applied to a specimen during a fracture-toughness test, t is the specimen thickness, a is the crack length, and w is the specimen width.

APPENDIX C

The following relationship was used for the elastic-plastic failure analysis (ref. 13):

$$K_F = \frac{K_{Ie}}{1 - m\left(\frac{S_n}{S_u}\right)} \qquad \left(S_n < S_u\right) \qquad \text{(C5)}$$

where K_F and m are two material fracture-toughness parameters, K_{Ie} is the elastic fracture toughness (elastic stress-intensity factor at failure), and S_n is the elastic nominal failure stress. The stress S_u is computed from the load required to produce a fully plastic region, or hinge, on the net section (based on the ultimate tensile strength σ_u). For the compact specimen, S_u is a function of load eccentricity (ref. 14) and is $1.62\sigma_u$ for $a/w = 0.5$.

The parameters K_F and m are assumed to be constant in the same sense as the ultimate tensile strength; that is, the parameters may vary with material thickness, state of stress, temperature, and rate of loading. To obtain fracture constants that are representative for a given material and test temperature, the fracture data should be from a single batch of material of the same thickness and from tests that encompass a wide range of specimen widths or crack lengths.

Fatigue-Crack Growth

The fatigue-crack-growth data were analyzed using procedures based on the stress-intensity factor. Numerous investigators (e.g., refs. 15 and 17) have demonstrated that the rate of fatigue-crack growth is a function of the stress-intensity range; that is,

$$\frac{da}{dN} = f_3(\Delta K) \qquad \text{(C6)}$$

where

$$\Delta K = K_{max} - K_{min} \qquad \text{(C7)}$$

for the specimen configurations used,

$$K_{max} = \left(\frac{P_{max}}{tw^{1/2}}\right) f_1\left(\frac{a}{w}\right) \qquad \text{(C8)}$$

and

$$K_{min} = \left(\frac{P_{min}}{tw^{1/2}}\right) f_1\left(\frac{a}{w}\right) \qquad \text{(C9)}$$

where equation (C2) gives $f_1\left(\frac{a}{w}\right)$.

APPENDIX C

Sustained-Load Flaw Growth

Stress-intensity analysis procedures were also used to analyze sustained-load flaw-growth data. For the 50.8-mm (2.0-in.) wide specimens, K_{Ii} is given by equation (C8). For the 91.4-mm (3.6-in.) wide specimens, K_{Ii} is given by

$$K_{Ii} = \left(\frac{P_{max}a^{1/2}}{tw}\right)f_4\left(\frac{a}{w}\right) \qquad \text{(C10)}$$

where figure 7 in reference 18 gives (in the present notation) $f_4\left(\frac{a}{w}\right)$.

REFERENCES

1. Damage Tolerant Design Handbook. HB-01, MCIC, Battelle Columbus Lab., Sept. 1973.
2. Ferrous. Part A of Section II-Material Specifications, ASME Boiler and Pressure Vessel Code, July 1, 1974.
3. Metric Practice Guide. E 380-72, American Soc. Testing Mater., June 1972.
4. Standard Specification for Pressure Vessel Plates, Alloy Steel, Manganese-Vanadium. ASTM Designation: A 225-72. Part 4 of 1974 Annual Book of ASTM Standards, 1974, pp. 140-141.
5. Standard Methods of Tension Testing of Metallic Materials. ASTM Designation: E 8-69. Part 10 of 1974 Annual Book of ASTM Standards, 1974, pp. 90-110.
6. Standard Method of Test for Plane-Strain Fracture Toughness of Metallic Materials. ASTM Designation: E 399-74. Part 10 of 1974 Annual Book of ASTM Standards, 1974, pp. 432-451.
7. Newman, J. C., Jr.: Stress Analysis of the Compact Specimen Including the Effects of Pin Loading. Fracture Analysis, Spec. Tech. Publ. 560, American Soc. Testing Mater., 1974, pp. 105-121.
8. Standard Methods for Notched Bar Impact Testing of Metallic Materials. ASTM Designation: E 23-72. Part 10 of 1974 Annual Book of ASTM Standards, 1974, pp. 167-183.
9. Standard Method for Conducting Drop-Weight Test To Determine Nil-Ductility Transition Temperature of Ferritic Steels. ASTM Designation: E 208-69. Part 10 of 1974 Annual Book of ASTM Standards, 1974, pp. 302-321.
10. Imig, L. A.: Effect of Initial Loads and of Moderately Elevated Temperature on the Room-Temperature Fatigue Life of Ti-8Al-1Mo-1V Titanium-Alloy Sheet. NASA TN D-4061, 1967.
11. Hudson, C. Michael: The Fatigue-Crack Growth and Fracture Characteristics of a Precipitation-Hardened Semiaustenitic Stainless Steel. M. S. Thesis, Virginia Polytech. Inst. & State Univ., Apr. 1965.
12. Grover, H. J.; Hyler, W. S.; Kuhn, Paul; Landers, Charles B.; and Howell, F. M.: Axial-Load Fatigue Properties of 24S-T and 75S-T Aluminum Alloy as Determined in Several Laboratories. NACA Rep. 1190, 1954. (Supersedes NACA TN 2928.)
13. Newman, J. C., Jr.: Fracture Analysis of Surface- and Through-Cracked Sheets and Plates. Eng. Fract. Mech., vol. 5, no. 3, Sept. 1973, pp. 667-689.

14. Newman, J. C., Jr.: Plane-Stress Fracture of Compact and Notch-Bend Specimens. NASA TM X-71926, 1974.

15. Barsom, J. M.: Fatigue-Crack Propagation in Steels of Various Yield Strengths. Trans. ASME, Ser. B: J. Eng. Ind., vol. 93, no. 4, Nov. 1971, pp. 1190-1196.

16. Fracture Toughness Testing and Its Applications. Spec. Tech. Publ. No. 381, American Soc. Testing Mater., Apr. 1965.

17. Paris, Paul C.: The Fracture Mechanics Approach to Fatigue. Fatigue – An Interdisciplinary Approach, John J. Burke, Norman L. Reed, and Volker Weiss, eds., Syracuse Univ. Press, 1964, pp. 107-132.

18. Wessel, E. T.: State of the Art of the WOL Specimen K_{Ic} Fracture Toughness Testing. Eng. Fract. Mech., vol. 1, no. 1, June 1968, pp. 77-103.

TABLE I.- TENSILE AND CHEMICAL PROPERTIES OF THE THREE STEELS TESTED

(a) Tensile

Steel	σ_u		σ_y		e, percent
	MPa	ksi	MPa	ksi	
VMS 5002	675	97.9	507	73.5	28
VMS 1146A	698	101.3	517	75.0	31
A-225 Gr.B	566	82.1	403	58.4	34

(b) Chemical[a]

Steel	C	Mn	P	S	Si	V	Ni	Fe
VMS 5002	0.23	1.45	0.015	0.023	0.30	0.15	0.59	Bal.
VMS 1146A	.21	1.31	.014	.024	.28	.15	.55	Bal.
A-225 Gr.B	.15	1.27	.013	.026	.27	.12	---	Bal.

[a]Values are in percent.

TABLE II.- FRACTURE-TOUGHNESS PROPERTIES OF THE THREE STEELS TESTED

t		w		T		a_i		P_f		K_{Ie}	
mm	in.	mm	in.	K	°F	mm	in.	kN	kips	$MN/m^{3/2}$	$ksi\text{-}in^{1/2}$
VMS 5002											
25.4	1.0	50.8	2.0	294	70	19.1	0.75	109.0	24.5	131	119
25.4	1.0	50.8	2.0	294	70	25.4	1.00	62.3	14.0	104	95
25.4	1.0	50.8	2.0	294	70	25.4	1.00	68.1	15.3	114	104
25.4	1.0	50.8	2.0	294	70	31.8	1.25	40.0	9.0	104	95
45.7	1.8	91.4	3.6	294	70	43.9	1.73	201.9	45.4	132	120
45.7	1.8	91.4	3.6	294	70	44.5	1.75	234.9	52.8	156	142
45.7	1.8	91.4	3.6	244	-20	44.2	1.74	186.8	42.0	123	112
45.7	1.8	91.4	3.6	244	-20	44.7	1.76	235.8	53.0	159	145
45.7	1.8	91.4	3.6	227	-50	43.4	1.71	217.5	48.9	141	128
45.7	1.8	91.4	3.6	227	-50	44.7	1.76	223.3	50.2	151	137
109.2	4.3	71.1	2.8	266	20	38.9	1.53	429.3	96.5	192	175
109.2	4.3	71.1	2.8	266	20	38.9	1.53	442.6	99.5	186	169
109.2	4.3	71.1	2.8	244	-20	38.9	1.53	373.7	84.0	163	148
VMS 1146A											
25.4	1.0	50.8	2.0	294	70	25.4	1.00	53.8	12.1	90	82
25.4	1.0	91.4	3.6	294	70	45.0	1.77	114.8	25.8	140	127
25.4	1.0	91.4	3.6	244	-20	44.7	1.76	120.1	27.0	145	132
25.4	1.0	91.4	3.6	227	-50	44.5	1.75	81.4	18.3	98	89
A-225 Gr.B											
25.4	1.0	50.8	2.0	294	70	25.4	1.00	53.4	12.0	90	82
25.4	1.0	50.8	2.0	294	70	25.4	1.00	50.3	11.3	84	76
45.7	1.8	91.4	3.6	294	70	44.5	1.75	200.2	45.0	133	121
45.7	1.8	91.4	3.6	294	70	44.7	1.76	193.1	43.4	130	118
45.7	1.8	91.4	3.6	244	-20	44.5	1.75	201.5	45.3	134	122
45.7	1.8	91.4	3.6	244	-20	44.5	1.75	193.5	43.5	130	118
83.8	3.3	71.1	2.8	266	20	46.2	1.82	226.9	51.0	129	117
83.8	3.3	71.1	2.8	266	20	46.2	1.82	231.3	52.0	131	119
83.8	3.3	71.1	2.8	244	-20	46.2	1.82	229.1	51.5	130	118
83.8	3.3	71.1	2.8	244	-20	46.2	1.82	236.7	53.2	134	122

TABLE III.- FATIGUE-CRACK-GROWTH DATA

ΔK		da/dN	
$MN/m^{3/2}$	$ksi\text{-}in^{1/2}$	nm/cycle	in/cycle
VMS 5002			
20.0	18.2	45.7	1.8×10^{-6}
21.1	19.2	30.5	1.2×10^{-6}
21.4	19.5	38.1	1.5×10^{-6}
21.9	19.9	30.5	1.2×10^{-6}
22.6	20.6	63.5	2.5×10^{-6}
22.9	20.8	35.6	1.4×10^{-6}
23.7	21.6	25.4	1.0×10^{-6}
24.2	22.0	73.7	2.9×10^{-6}
24.5	22.3	86.4	3.4×10^{-6}
24.7	22.5	50.8	2.0×10^{-6}
24.8	22.6	43.2	1.7×10^{-6}
25.5	23.2	111.8	4.4×10^{-6}
26.0	23.7	40.6	1.6×10^{-6}
26.3	23.9	58.4	2.3×10^{-6}
26.5	24.1	73.7	2.9×10^{-6}
27.0	24.6	99.1	3.9×10^{-6}
27.6	25.1	66.0	2.6×10^{-6}
28.0	25.5	142.2	5.6×10^{-6}
28.1	25.6	68.6	2.7×10^{-6}
28.8	26.2	127.0	5.0×10^{-6}
29.5	26.8	91.4	3.6×10^{-6}
29.8	27.1	147.3	5.8×10^{-6}
29.9	27.2	111.8	4.4×10^{-6}
30.1	27.4	61.0	2.4×10^{-6}
30.2	27.5	221.0	8.7×10^{-6}
30.9	28.1	61.0	2.4×10^{-6}
31.2	28.4	157.5	6.2×10^{-6}
31.4	28.6	119.4	4.7×10^{-6}
32.0	29.1	185.4	7.3×10^{-6}
32.2	29.3	205.7	8.1×10^{-6}
32.3	29.4	127.0	5.0×10^{-6}
32.5	29.6	190.5	7.5×10^{-6}
33.2	30.2	304.8	1.2×10^{-5}
33.4	30.4	101.6	4.0×10^{-6}
34.2	31.1	144.8	5.7×10^{-6}
34.3	31.2	304.8	1.2×10^{-5}
34.6	31.5	381.0	1.5×10^{-5}
34.6	31.5	254.0	1.0×10^{-5}
35.7	32.5	78.7	3.1×10^{-6}
35.9	32.7	165.1	6.5×10^{-6}
36.3	33.0	279.4	1.1×10^{-5}
36.4	33.1	685.8	2.7×10^{-5}
36.5	33.2	152.4	6.0×10^{-6}
36.5	33.2	78.7	3.1×10^{-6}
37.0	33.7	111.8	4.4×10^{-6}
37.4	34.0	381.0	1.5×10^{-5}
38.6	35.1	68.6	2.7×10^{-6}
39.6	36.0	228.6	9.0×10^{-6}
39.8	36.1	180.3	7.1×10^{-6}
40.1	36.5	142.2	5.6×10^{-6}
41.8	38.0	406.4	1.6×10^{-5}
42.9	39.0	431.8	1.7×10^{-5}
43.0	39.1	609.6	2.4×10^{-5}
43.7	39.8	228.6	9.0×10^{-6}
44.3	40.3	233.7	9.2×10^{-6}
46.3	42.1	584.2	2.3×10^{-5}
47.7	43.4	203.2	8.0×10^{-6}
47.8	43.5	609.6	2.4×10^{-5}
48.9	44.5	787.4	3.1×10^{-5}
50.0	45.5	711.2	2.8×10^{-5}
51.8	47.1	939.8	3.7×10^{-5}
52.2	47.5	889.0	3.5×10^{-5}
55.4	50.4	965.2	3.8×10^{-5}
56.1	51.0	584.2	2.3×10^{-5}
56.4	51.3	609.6	2.4×10^{-5}
57.1	52.0	889.0	3.5×10^{-5}
58.2	53.0	1219.2	4.8×10^{-5}
59.1	53.8	1320.8	5.2×10^{-5}
60.2	54.8	838.2	3.3×10^{-5}
62.6	57.0	1270.0	5.0×10^{-5}
63.4	57.7	1371.6	5.4×10^{-5}
64.6	58.8	711.2	2.8×10^{-5}
66.5	60.5	1117.6	4.4×10^{-5}
68.5	62.3	990.6	3.9×10^{-5}
68.7	62.5	1981.2	7.8×10^{-5}
70.1	63.8	2082.8	8.2×10^{-5}
72.8	66.2	2794.0	1.1×10^{-4}

TABLE III.- Continued

ΔK		da/dN	
$MN/m^{3/2}$	$ksi\text{-}in^{1/2}$	nm/cycle	in/cycle
VMS 1146A			
30.2	27.5	254.0	1.0×10^{-5}
32.3	29.4	304.8	1.2×10^{-5}
32.3	29.4	330.2	1.3×10^{-5}
34.1	31.0	381.0	1.5×10^{-5}
34.6	31.5	406.4	1.6×10^{-5}
36.3	33.0	508.0	2.0×10^{-5}
36.8	33.5	482.6	1.9×10^{-5}
38.4	34.9	147.3	5.8×10^{-6}
39.0	35.5	482.6	1.9×10^{-5}
39.0	35.5	609.6	2.4×10^{-5}
40.4	36.8	457.2	1.8×10^{-5}
41.4	37.7	210.8	8.3×10^{-6}
41.8	38.0	457.2	1.8×10^{-5}
41.8	38.0	558.8	2.2×10^{-5}
42.6	38.8	144.8	5.7×10^{-6}
44.5	40.5	482.6	1.9×10^{-5}
44.5	40.5	914.4	3.6×10^{-5}
44.7	40.7	279.4	1.1×10^{-5}
47.8	43.5	1016.0	4.0×10^{-5}
47.8	43.5	1219.2	4.8×10^{-5}
48.0	43.7	381.0	1.5×10^{-5}
51.9	47.2	965.2	3.8×10^{-5}
51.9	47.2	1117.6	4.4×10^{-5}
52.5	47.8	457.2	1.8×10^{-5}
57.6	52.4	482.6	1.9×10^{-5}
64.5	58.7	787.4	3.1×10^{-5}

TABLE III.- Concluded

ΔK		da/dN	
$MN/m^{3/2}$	$ksi\text{-}in^{1/2}$	nm/cycle	in/cycle
A-225 Gr.B			
24.2	22.0	30.5	1.2×10^{-6}
25.6	23.3	50.8	2.0×10^{-6}
27.7	25.2	109.2	4.3×10^{-6}
30.2	27.5	119.4	4.7×10^{-6}
30.2	27.5	121.9	4.8×10^{-6}
30.2	27.5	132.1	5.2×10^{-6}
31.9	29.0	111.8	4.4×10^{-6}
31.9	29.0	121.9	4.8×10^{-6}
31.9	29.0	172.7	6.8×10^{-6}
32.9	29.9	91.4	3.6×10^{-6}
34.1	31.0	180.3	7.1×10^{-6}
34.1	31.0	213.4	8.4×10^{-6}
34.1	31.0	279.4	1.1×10^{-5}
36.3	33.0	152.4	6.0×10^{-6}
36.3	33.0	165.1	6.5×10^{-6}
36.3	33.0	228.6	9.0×10^{-6}
36.6	33.3	119.4	4.7×10^{-6}
36.7	33.4	152.4	6.0×10^{-6}
37.3	33.9	233.7	9.2×10^{-6}
37.9	34.5	198.1	7.8×10^{-6}
38.8	35.3	254.0	1.0×10^{-5}
38.8	35.3	381.0	1.5×10^{-5}
38.8	35.3	431.8	1.7×10^{-5}
38.9	35.4	248.9	9.8×10^{-6}
39.7	36.1	254.0	1.0×10^{-5}
40.3	36.7	241.3	9.5×10^{-6}
40.7	37.0	165.1	6.5×10^{-6}
41.5	37.8	279.4	1.1×10^{-5}
41.5	37.8	482.6	1.9×10^{-5}
41.5	37.8	812.8	3.2×10^{-5}
42.0	38.2	279.4	1.1×10^{-5}
42.9	39.0	304.8	1.2×10^{-5}
43.9	39.9	132.1	5.2×10^{-6}
44.0	40.0	175.3	6.9×10^{-6}
44.5	40.5	213.4	8.4×10^{-6}
44.5	40.5	304.8	1.2×10^{-5}
44.5	40.5	381.0	1.5×10^{-5}
46.0	41.9	355.6	1.4×10^{-5}
47.8	43.5	218.4	8.6×10^{-6}
47.8	43.5	508.0	2.0×10^{-5}
47.8	43.5	635.0	2.5×10^{-5}
47.9	43.6	330.2	1.3×10^{-5}
49.8	45.3	355.6	1.4×10^{-5}
52.2	47.5	381.0	1.5×10^{-5}
52.2	47.5	406.4	1.6×10^{-5}
52.2	47.5	482.6	1.9×10^{-5}
52.6	47.9	355.6	1.4×10^{-5}
54.5	49.6	609.6	2.4×10^{-5}
59.6	54.2	660.4	2.6×10^{-5}
65.0	59.1	939.8	3.7×10^{-5}
65.3	59.4	1701.8	6.7×10^{-5}
66.7	60.7	965.2	3.8×10^{-5}
67.4	61.3	609.6	2.4×10^{-5}
71.9	65.4	1346.2	5.3×10^{-5}

TABLE IV.- SUSTAINED-LOAD FLAW-GROWTH DATA

Test fluid	w		a_{sl}		P_{max}		K_{Ii}		Test duration		Results
	mm	in.	mm	in.	kN	kips	$MN/m^{3/2}$	$ksi\text{-}in^{1/2}$	ks	hr	
VMS 5002											
Air	91.4	3.6	48.8	1.92	85.4	19.2	101	92	421	117	NFG
	91.4	3.6	50.3	1.98	83.2	18.7	102	93	432	120	NFG
	91.4	3.6	49.5	1.95	86.7	19.5	106	96	450	125	NFG
	91.4	3.6	46.2	1.82	96.5	21.7	107	97	407	113	NFG
Distilled H_2O	50.8	2.0	25.4	1.00	46.7	10.5	79	72	2052	570	NFG
	91.4	3.6	49.8	1.96	84.5	19.0	103	94	407	113	NFG
	91.4	3.6	50.3	1.98	84.1	18.9	103	94	407	113	NFG
	91.4	3.6	49.3	1.94	86.7	19.5	104	95	407	113	NFG
	91.4	3.6	49.5	1.95	86.7	19.5	106	96	407	113	NFG
Distilled H_2O plus rust inhibitor	50.8	2.0	25.4	1.00	46.7	10.5	79	72	>3600	>1000	NFG
VMS 1146A											
Air	50.8	2.0	25.4	1.00	40.0	9.0	67	61	2592	720	NFG
	50.8	2.0	25.4	1.00	46.7	10.5	79	72	2592	720	NFG
	91.4	3.6	48.5	1.91	47.6	10.7	79	72	598	166	NFG
Distilled H_2O	50.8	2.0	25.4	1.00	46.7	10.5	79	72	2052	570	NFG
	91.4	3.6	46.2	1.82	51.6	11.6	79	72	598	166	NFG
Distilled H_2O plus rust inhibitor	50.8	2.0	25.4	1.00	46.7	10.5	79	72	>3600	>1000	NFG
A-225 Gr.B											
Air	50.8	2.0	25.4	1.00	40.0	9.0	67	61	2592	720	NFG
	50.8	2.0	25.4	1.00	46.7	10.5	79	72	4	1	Failed
	91.4	3.6	48.3	1.90	66.3	14.9	78	71	425	118	NFG
	91.4	3.6	49.3	1.94	64.9	14.6	78	71	428	119	NFG
Distilled H_2O	50.8	2.0	25.4	1.00	46.7	10.5	79	72	43	12	Failed
	91.4	3.6	46.7	1.84	68.1	15.3	77	70	425	118	NFG
	91.4	3.6	46.2	1.82	73.0	16.4	81	74	425	118	NFG
Distilled H_2O plus rust inhibitor	50.8	2.0	25.4	1.00	46.7	10.5	79	72	>3600	>1000	NFG

TABLE V.- CHARPY IMPACT DATA

T		C_{VN}		l_e	
K	°F	N-m	ft-lbf	mm	in.
VMS 5002					
311	100	72	53	0.71	0.028
297	75	88	65	1.12	.044
283	50	61	45	.79	.031
283	50	34	25	.41	.016
266	20	46	34	.56	.022
255	0	22	16	.28	.011
244	-20	34	25	.41	.016
239	-30	14	10	.08	.003
227	-50	24	18	.28	.011
227	-50	20	15	.23	.009
VMS 1146A					
339	150	132	97	1.17	0.046
311	100	122	90	1.14	.045
297	75	107	79	.97	.038
266	20	68	50	.86	.034
255	0	47	35	.53	.021
244	-20	56	41	.69	.027
239	-30	18	13	.20	.008
233	-40	24	18	.33	.013
227	-50	42	31	.56	.022
197	-105	14	10	.18	.007
A-225 Gr.B					
366	200	47	35	0.79	0.031
311	100	52	38	.94	.037
297	75	56	41	.84	.033
266	20	37	27	.64	.025
255	0	34	25	.69	.027
244	-20	27	20	.38	.015
239	-30	27	20	.43	.017
233	-40	31	23	.46	.018
227	-50	27	20	.43	.017

TABLE VI.- DROP-WEIGHT DATA

T		Test results	NDT	
K	°F		K	°F
VMS 5002				
255	0	Specimen survived		
255	0	Specimen survived		
255	0	Specimen survived		
250	-10	Specimen survived		
250	-10	Specimen failed	250	-10
244	-20	Specimen failed		
241	-25	Specimen failed		
227	-50	Specimen failed		
A-225 Gr.B				
255	0	Specimen survived		
247	-15	Specimen survived		
247	-15	Specimen survived		
241	-25	Specimen failed	241	-25
236	-35	Specimen failed		
227	-50	Specimen failed		

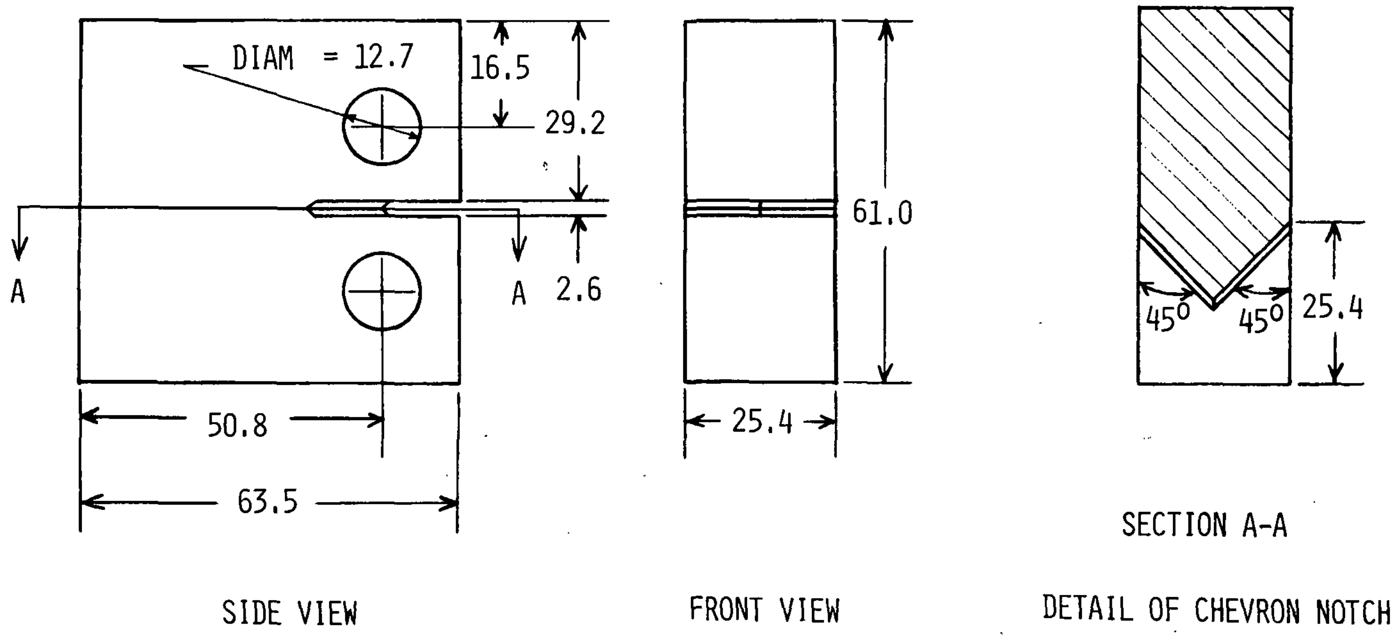

(a) w = 50.8 mm.

Figure 1.- Compact specimen configuration. All dimensions in mm.

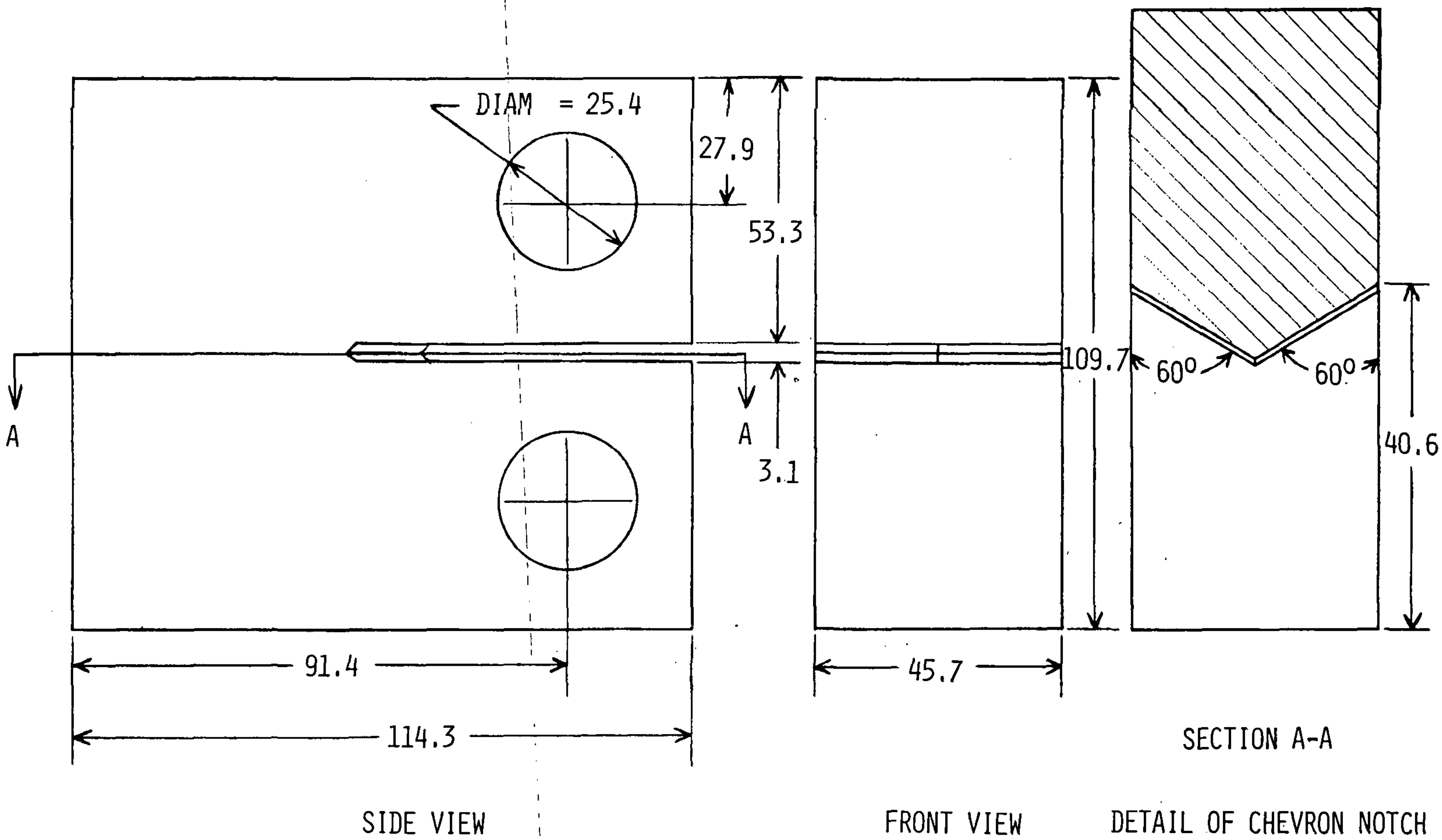

(b) w = 91.4 mm.

Figure 1.- Continued.

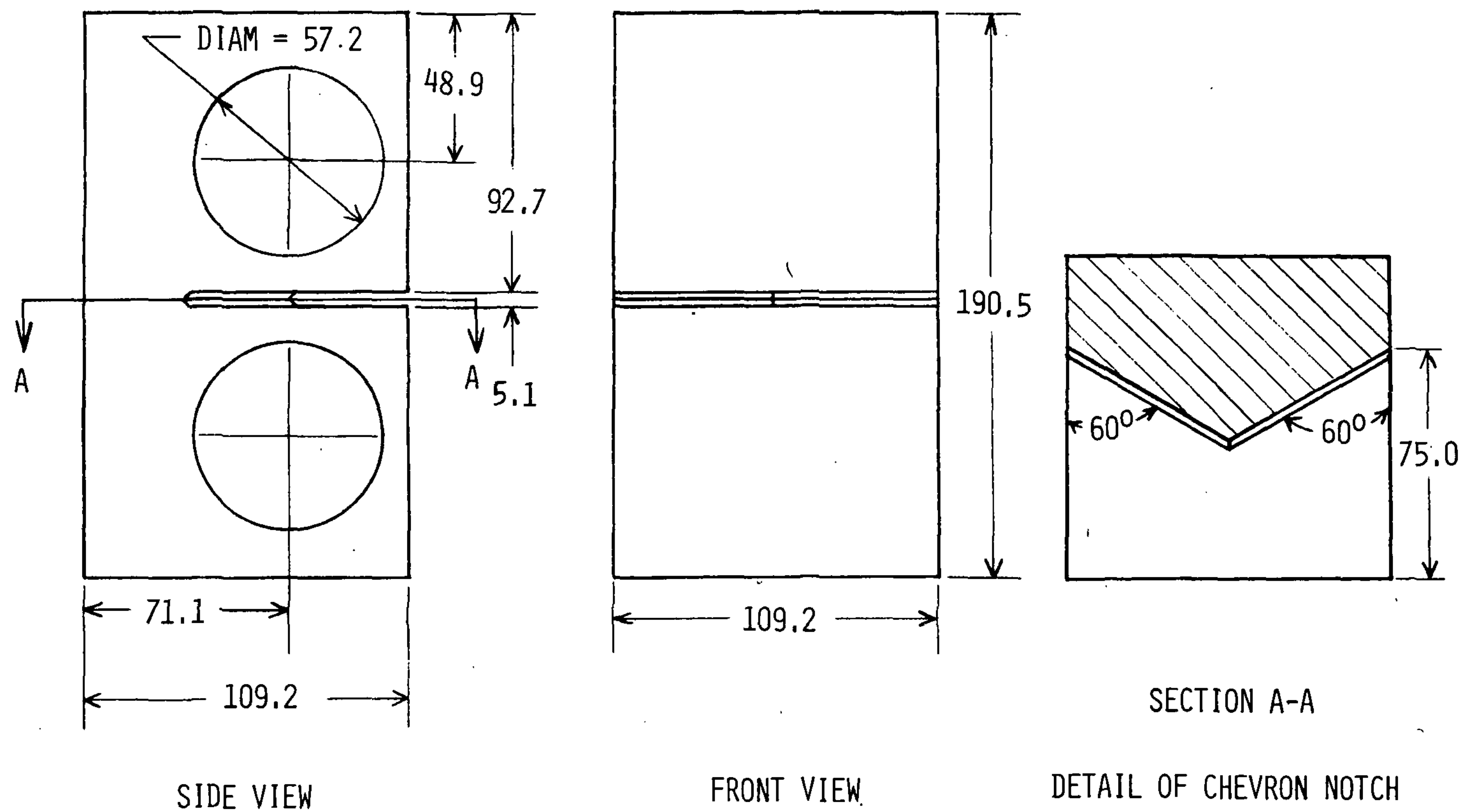

(c) w = 71.1 mm.

Figure 1.- Concluded.

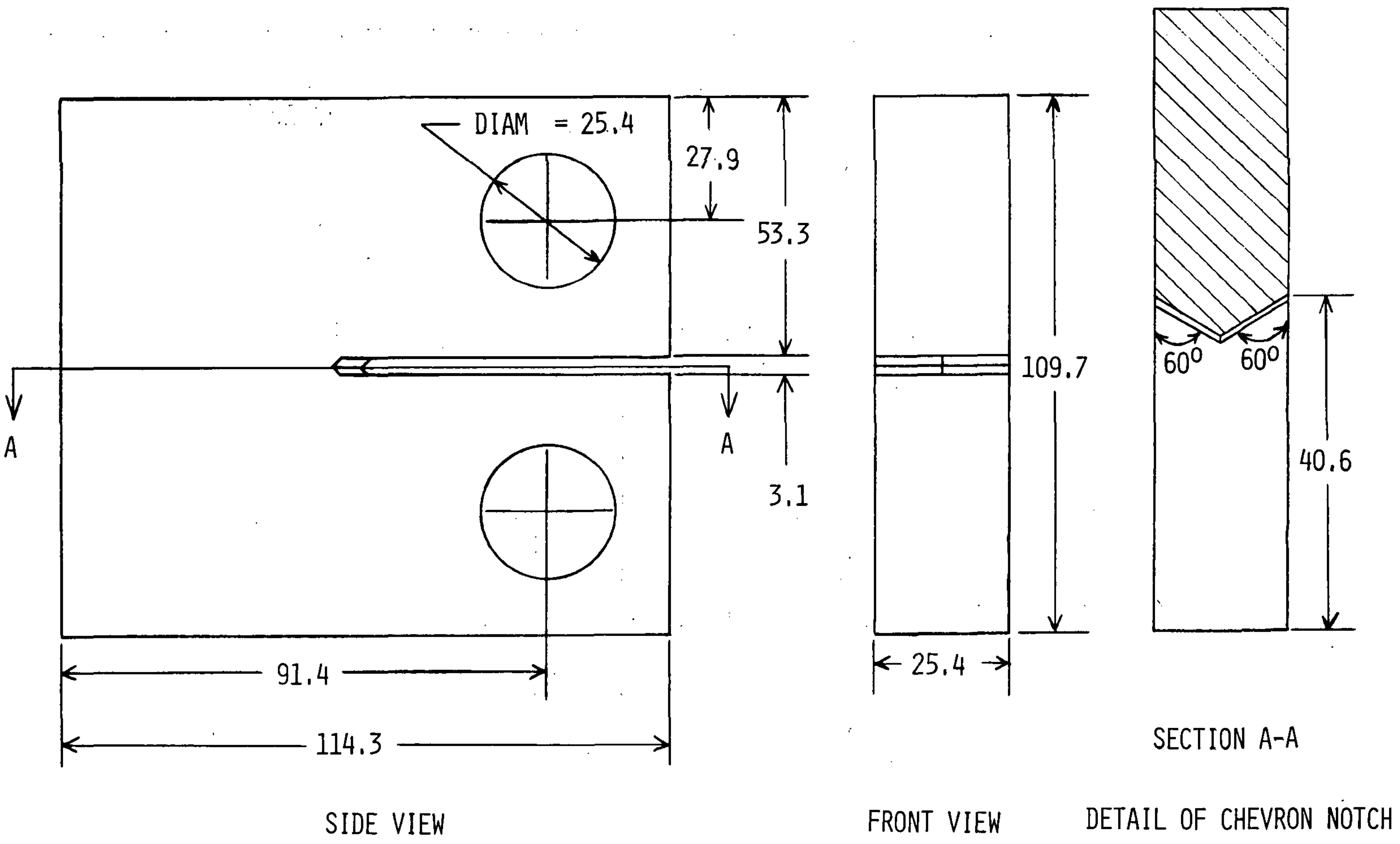

Figure 2.- Compact specimen configuration. All dimensions in mm. Specimen width, 91.4 mm.

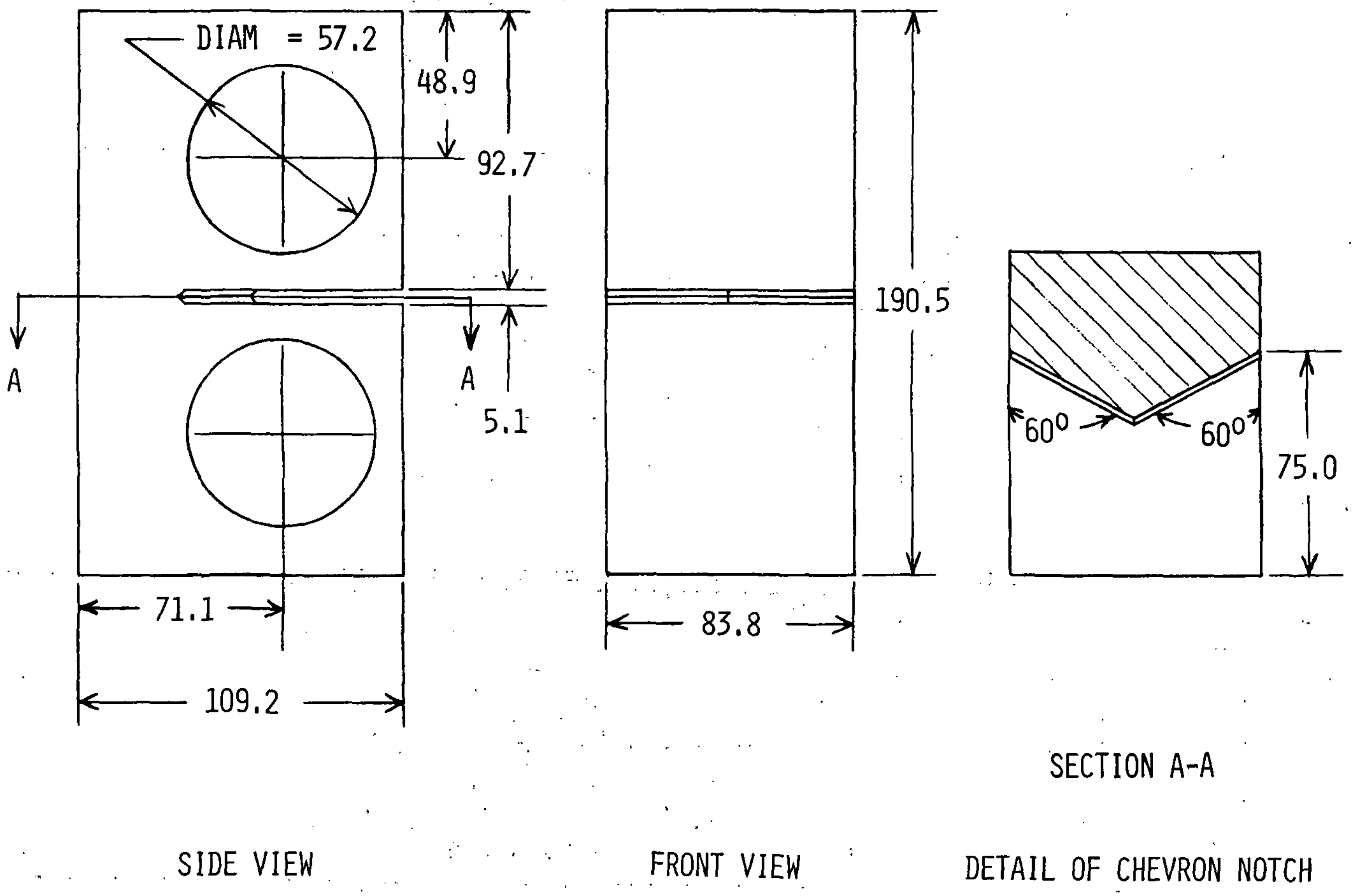

Figure 3.- Compact specimen configuration. All dimensions in mm. Specimen width, 71.1 mm.

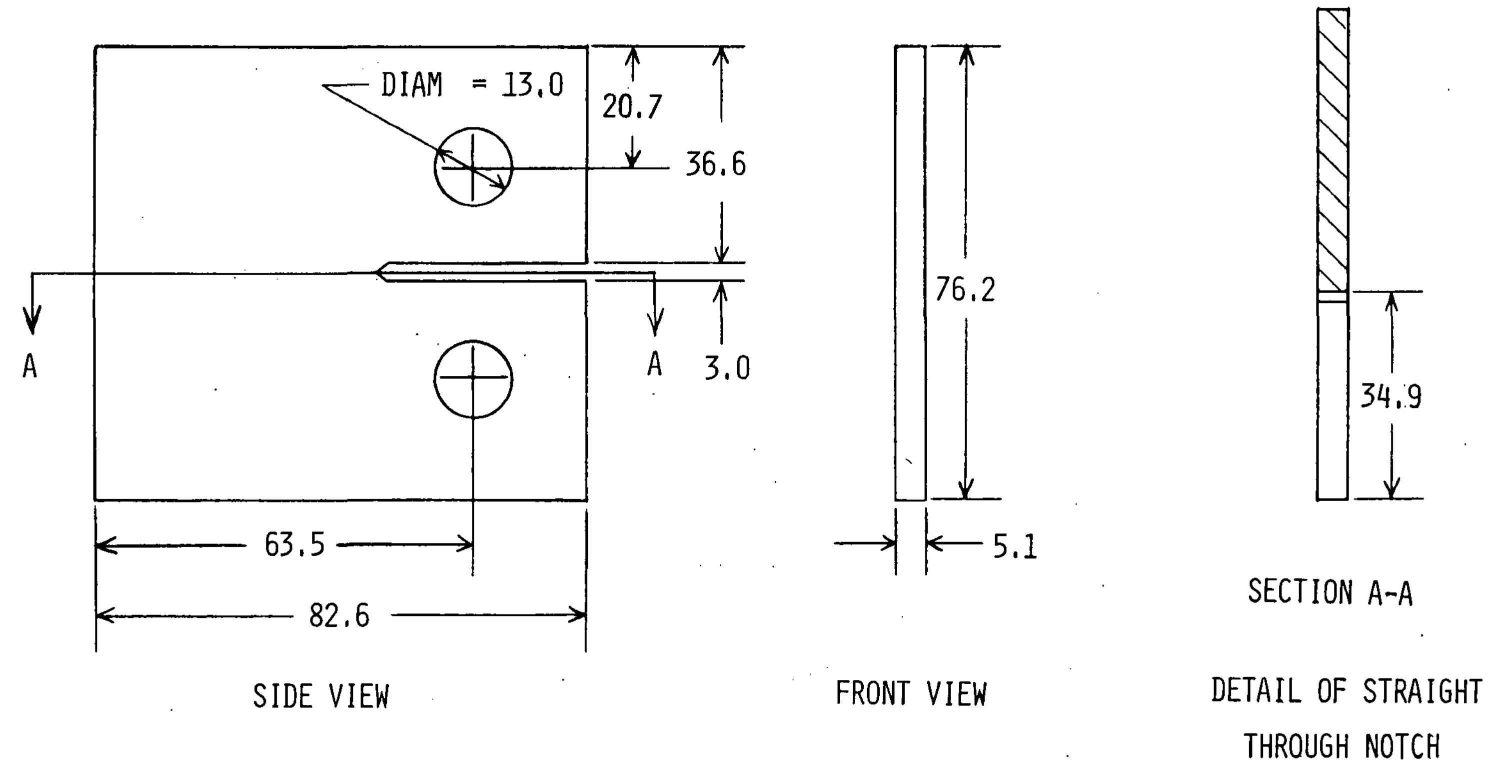

Figure 4.- Compact specimen configuration. All dimensions in mm. Specimen width, 63.5 mm.

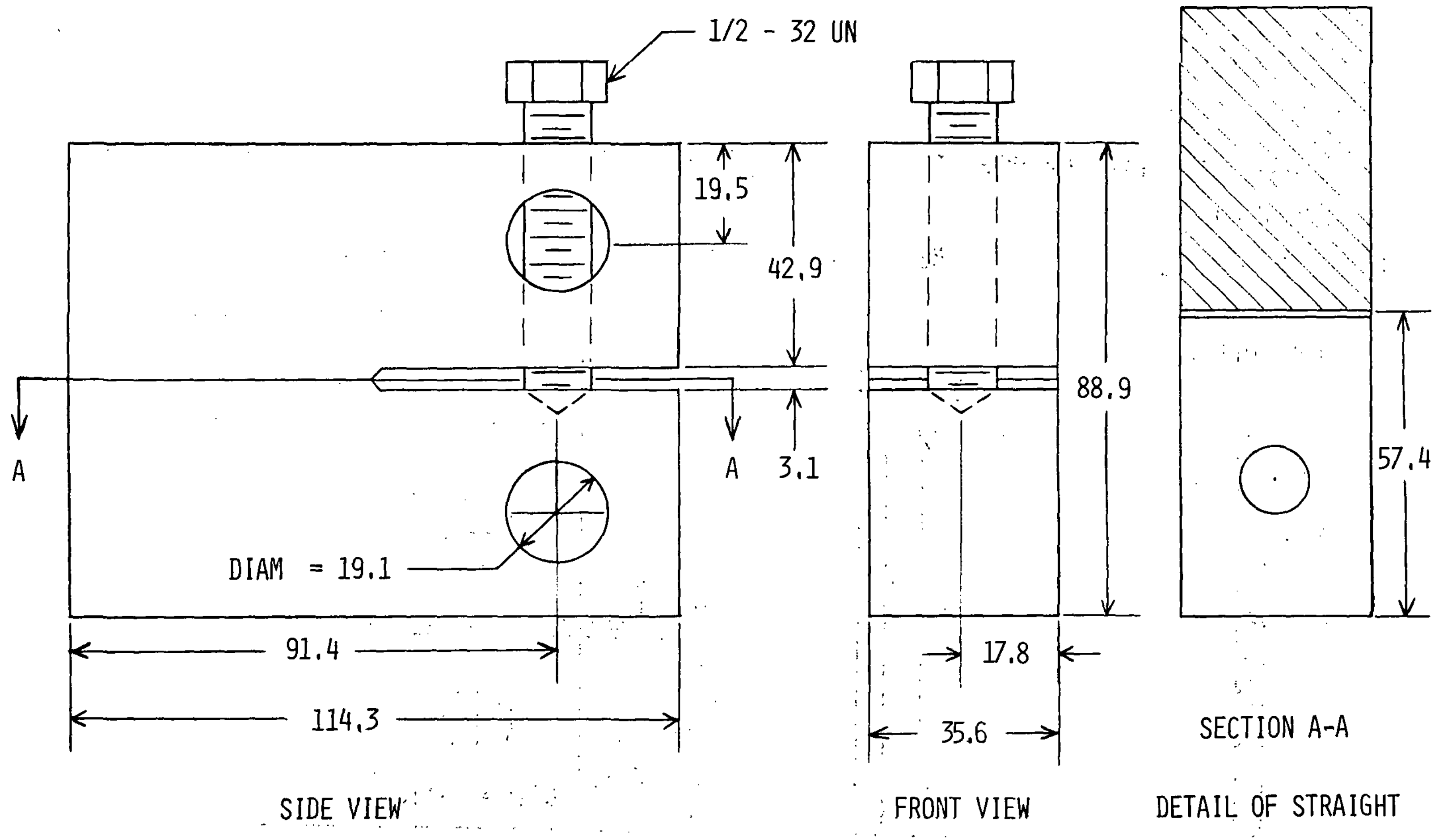

(a) t = 35.6 mm.

Figure 5.- Wedge-opening-load (WOL) specimen configuration. All dimensions, except screw designation, in mm.

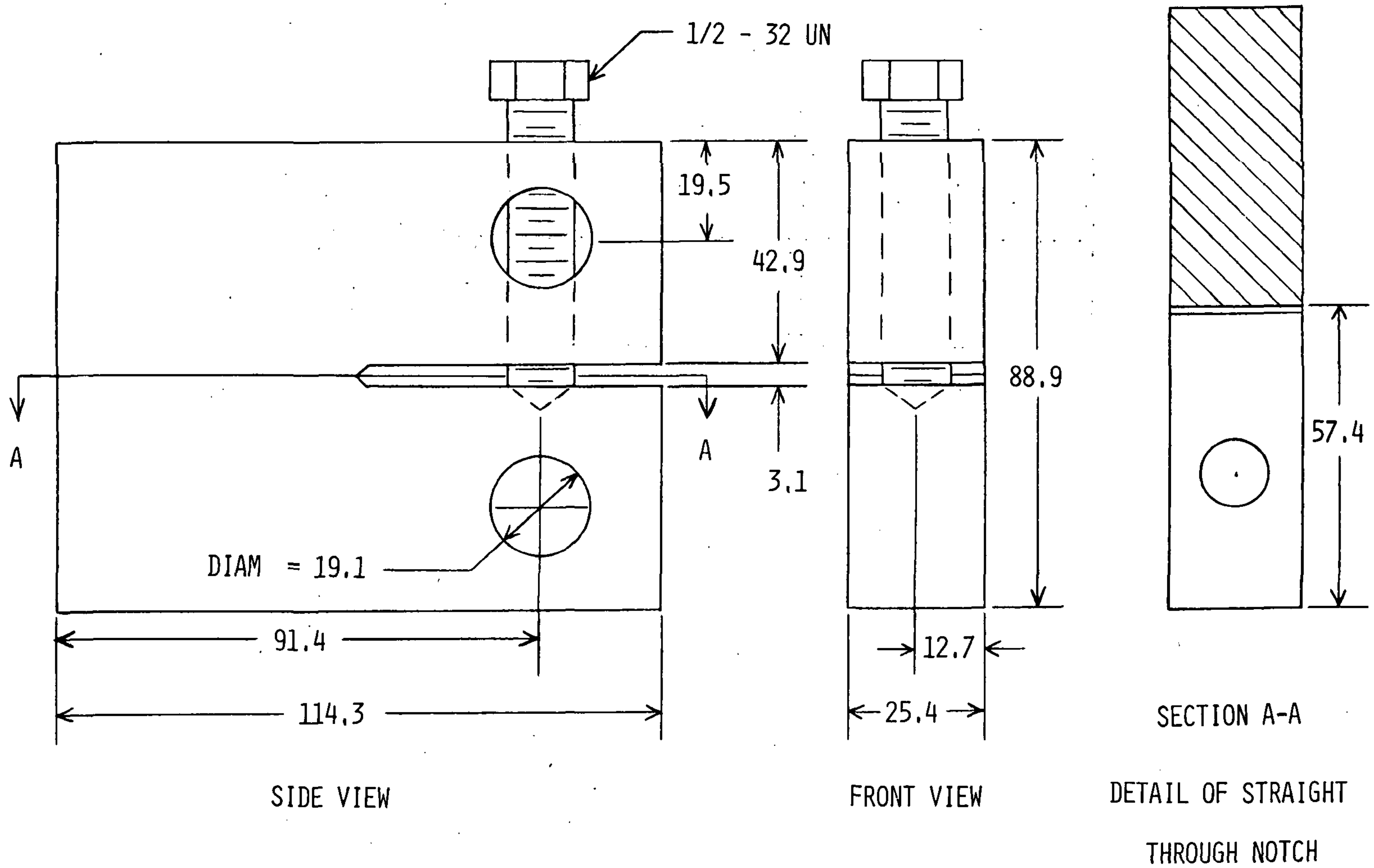

(b) t = 25.4 mm.

Figure 5.- Concluded.

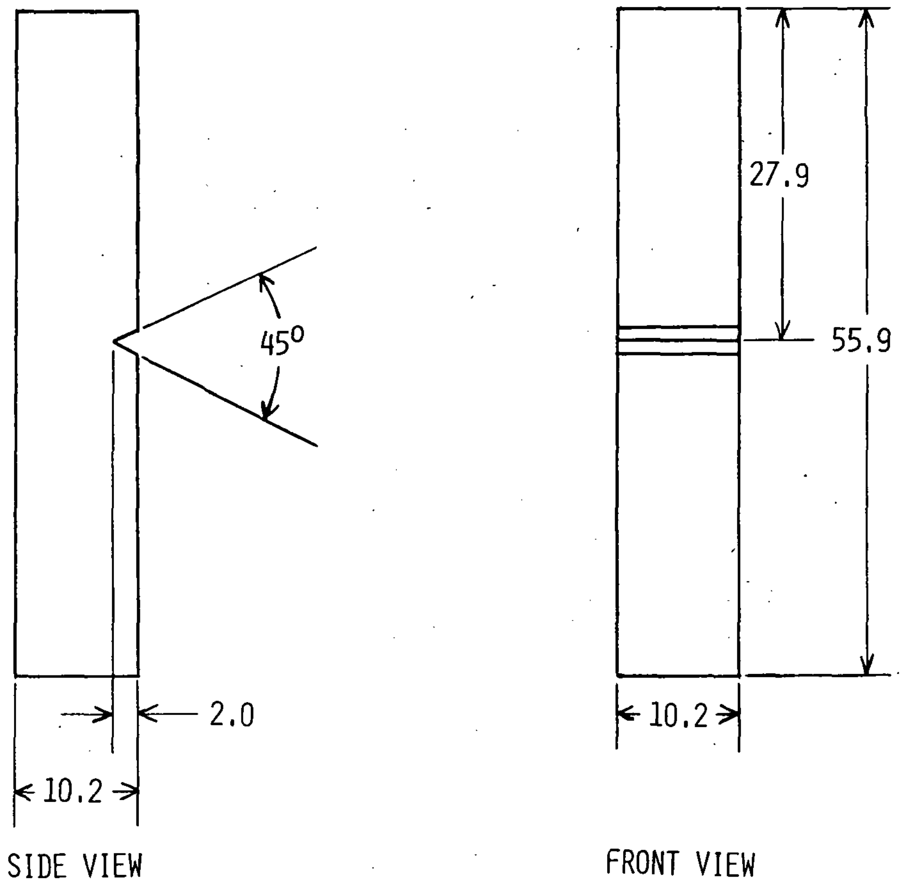

Figure 6.- Charpy V-notch specimen configuration. All dimensions in mm.

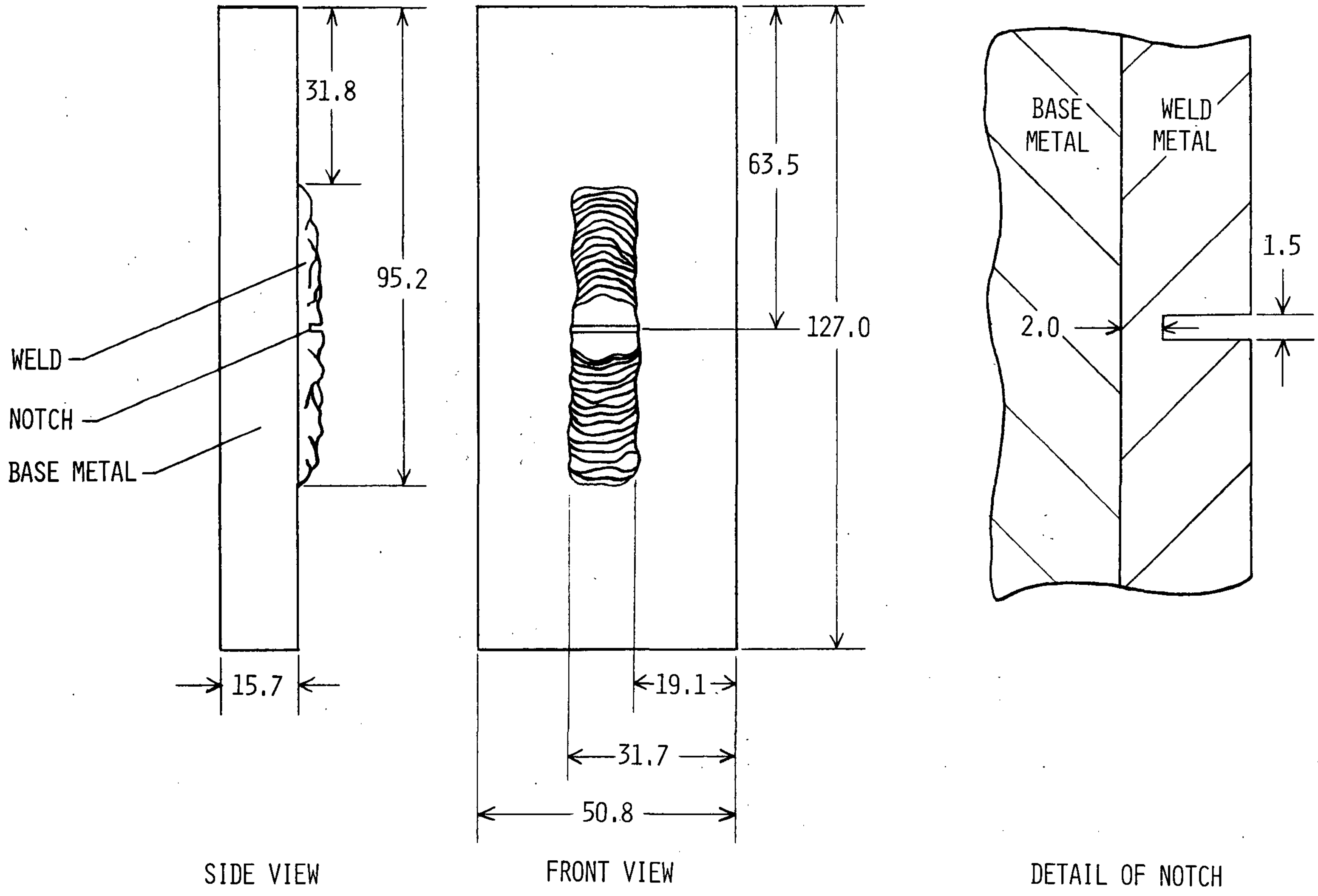

Figure 7.- Drop-weight specimen configuration. All dimensions in mm.

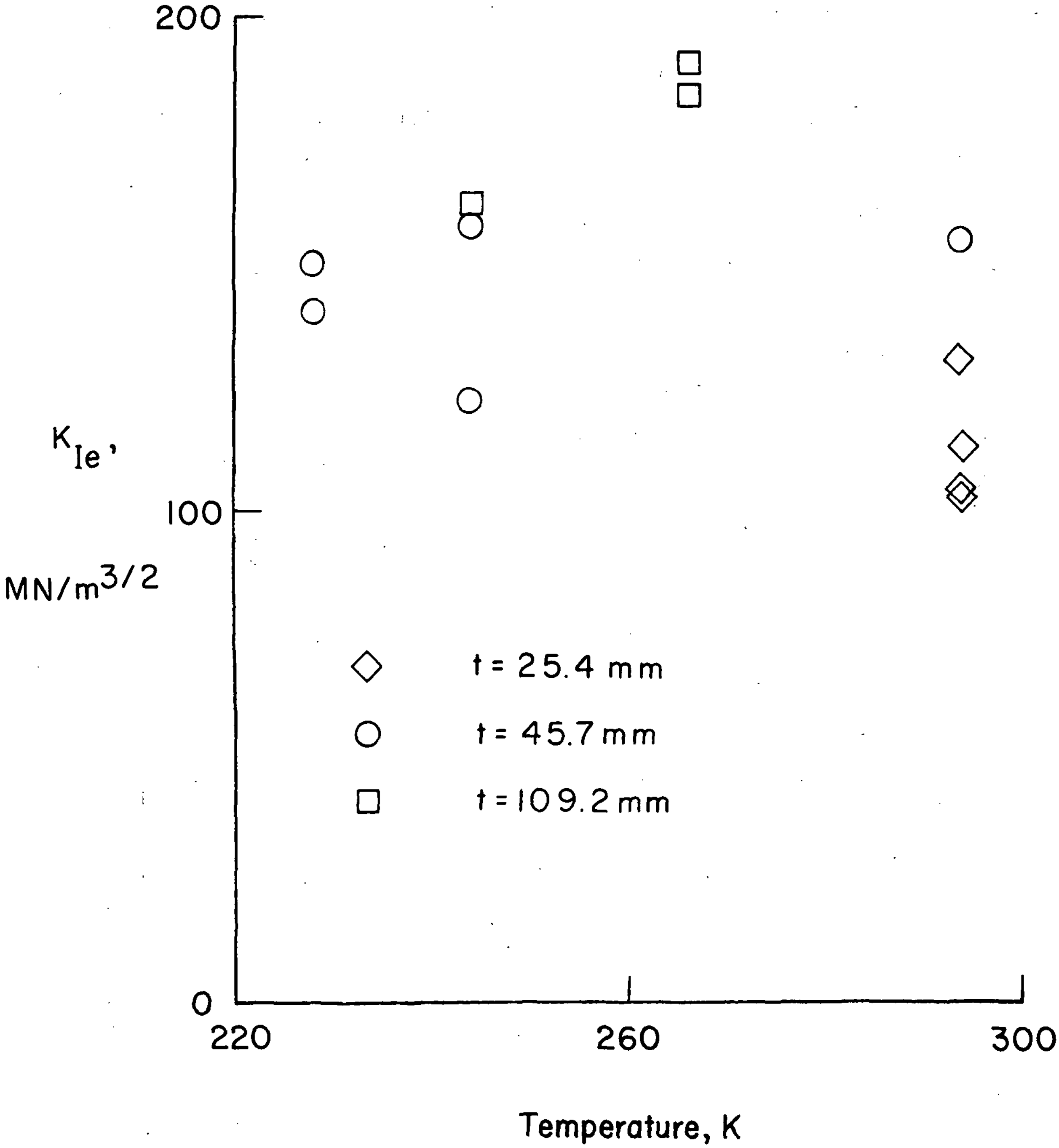

Figure 8.- Variation of K_{Ie} with temperature for VMS 5002 steel.

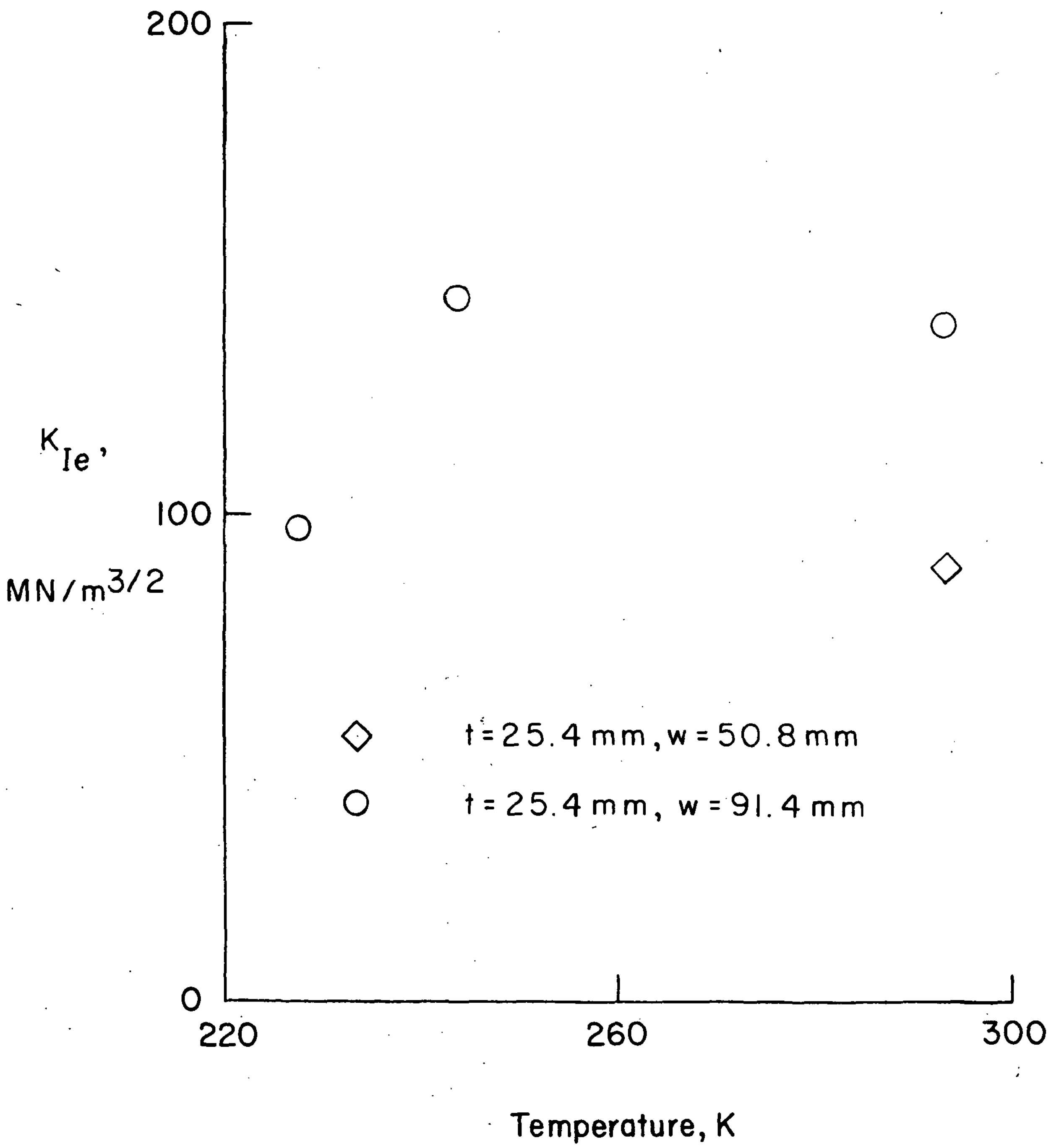

Figure 9.- Variation of K_{Ie} with temperature for VMS 1146A steel.

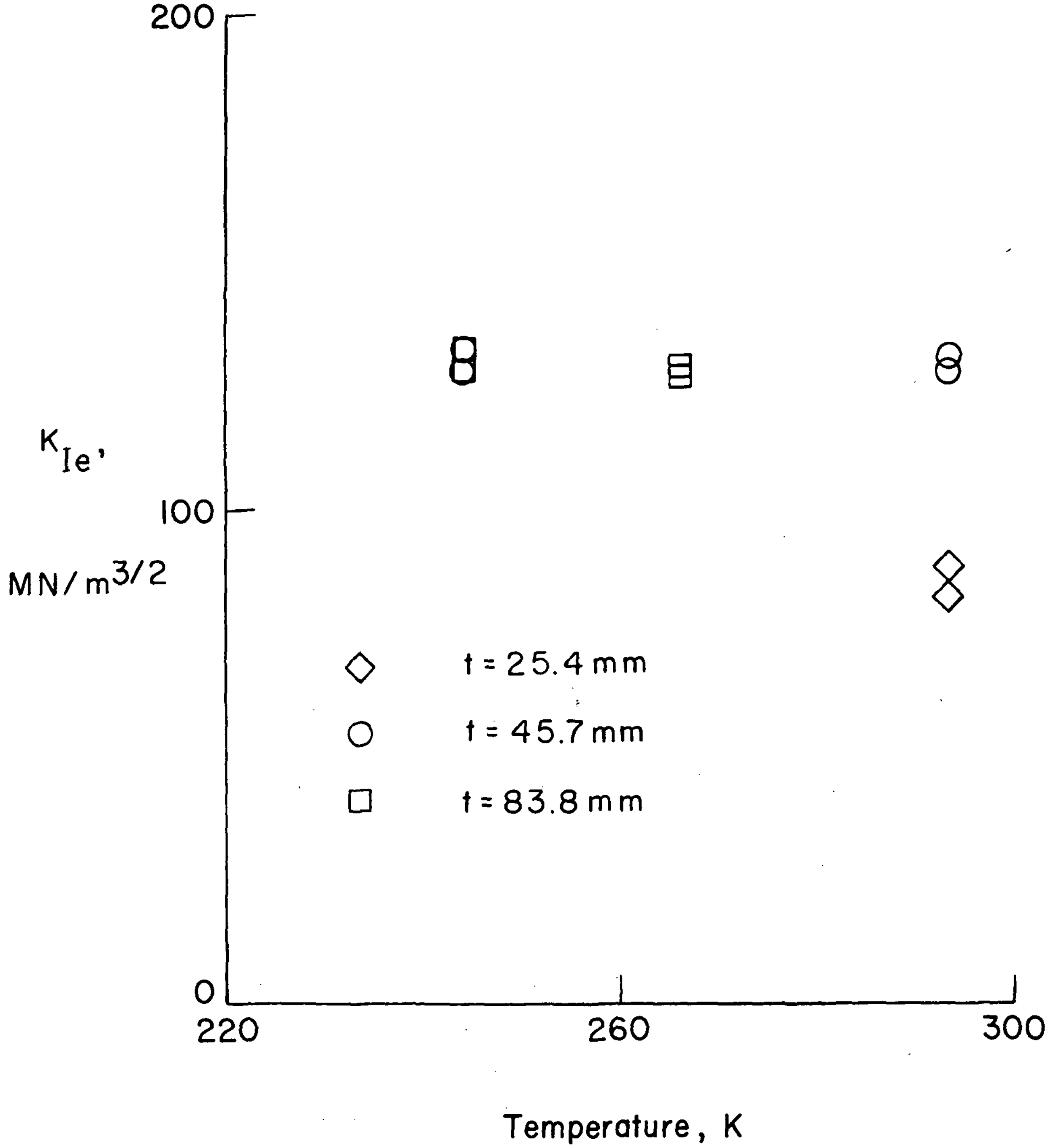

Figure 10.- Variation of K_{Ie} with temperature for A-225 Gr.B steel.

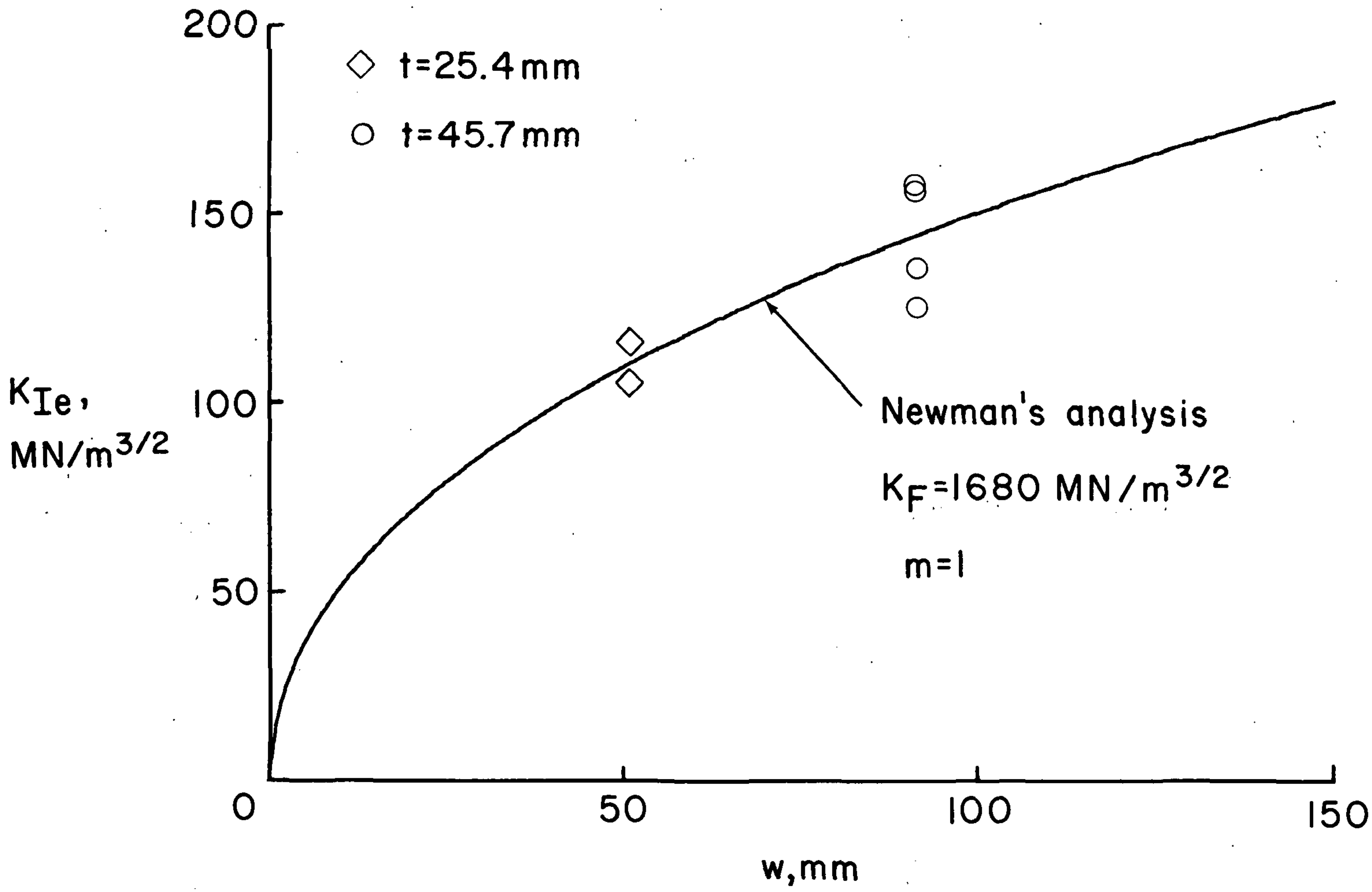

Figure 11.- Variation of K_{Ie} with specimen width for VMS 5002 steel. a/w = 0.5.

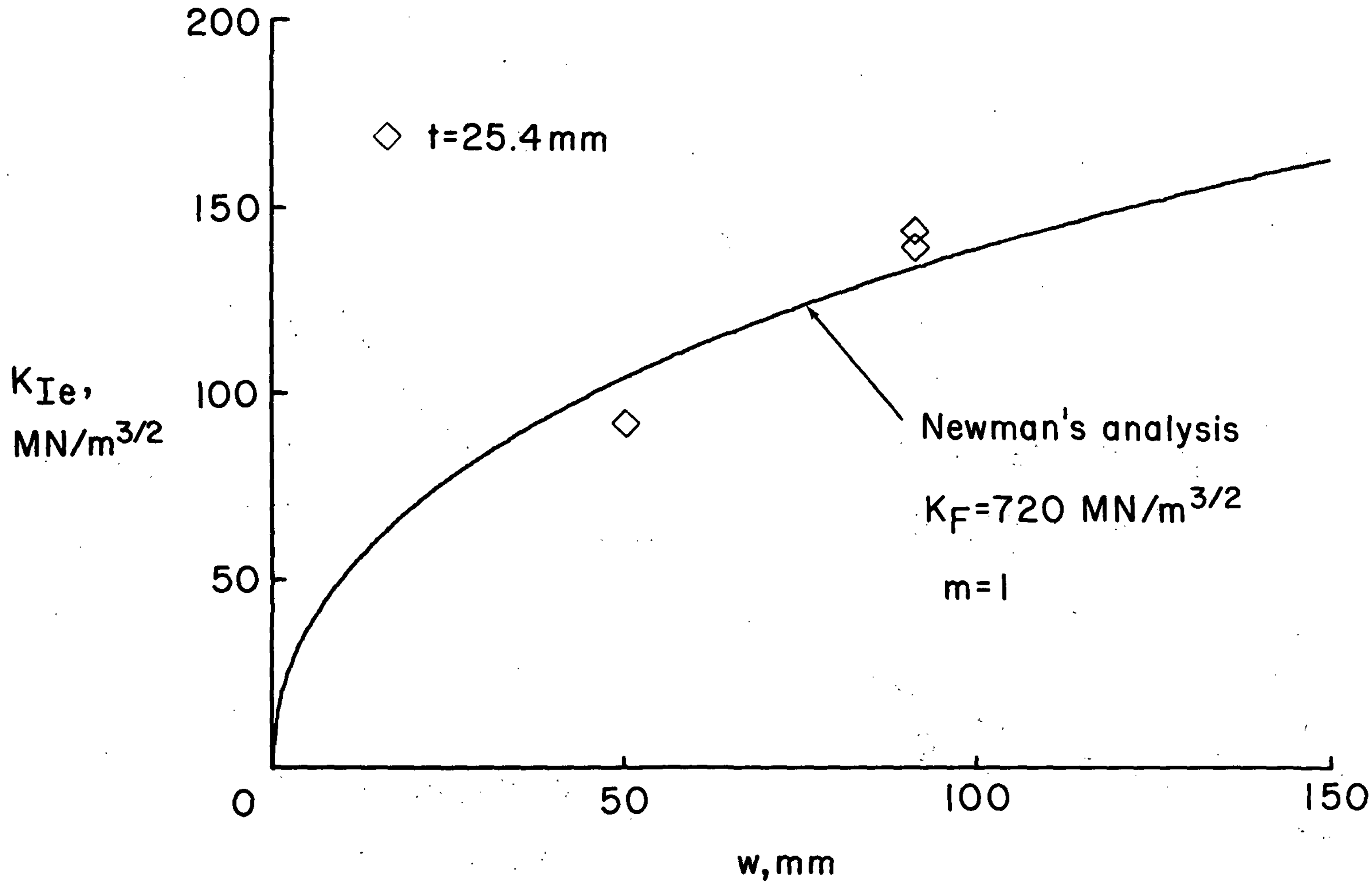

Figure 12.- Variation of K_{Ie} with specimen width for VMS 1146A. $a/w = 0.5$.

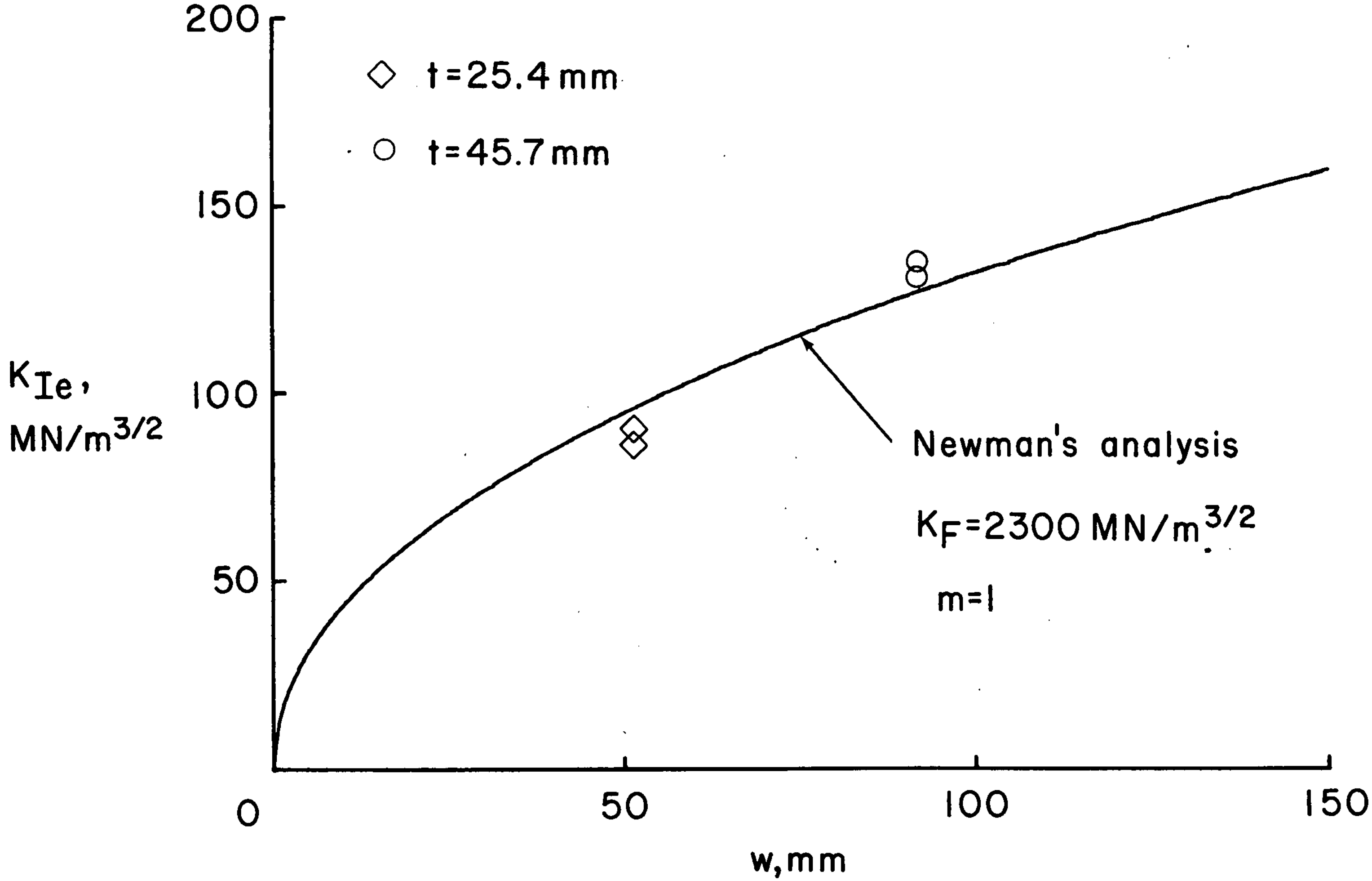

Figure 13.- Variation of K_{Ie} with specimen width for A-225 Gr.B. a/w = 0.5.

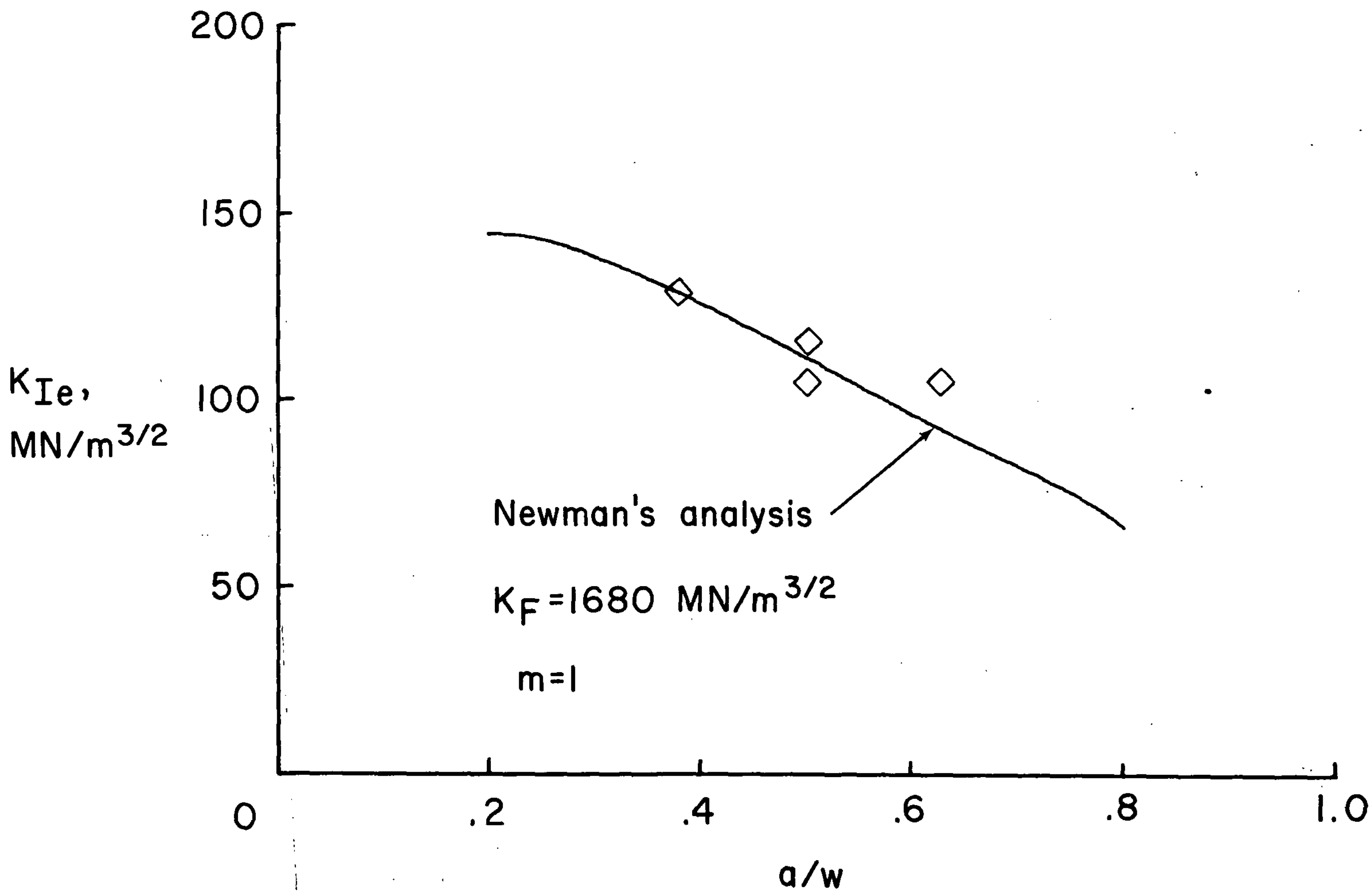

Figure 14.- Variation of K_{Ie} with a/w for the 25.4-mm-thick VMS 5002 specimens. w = 50.8 mm.

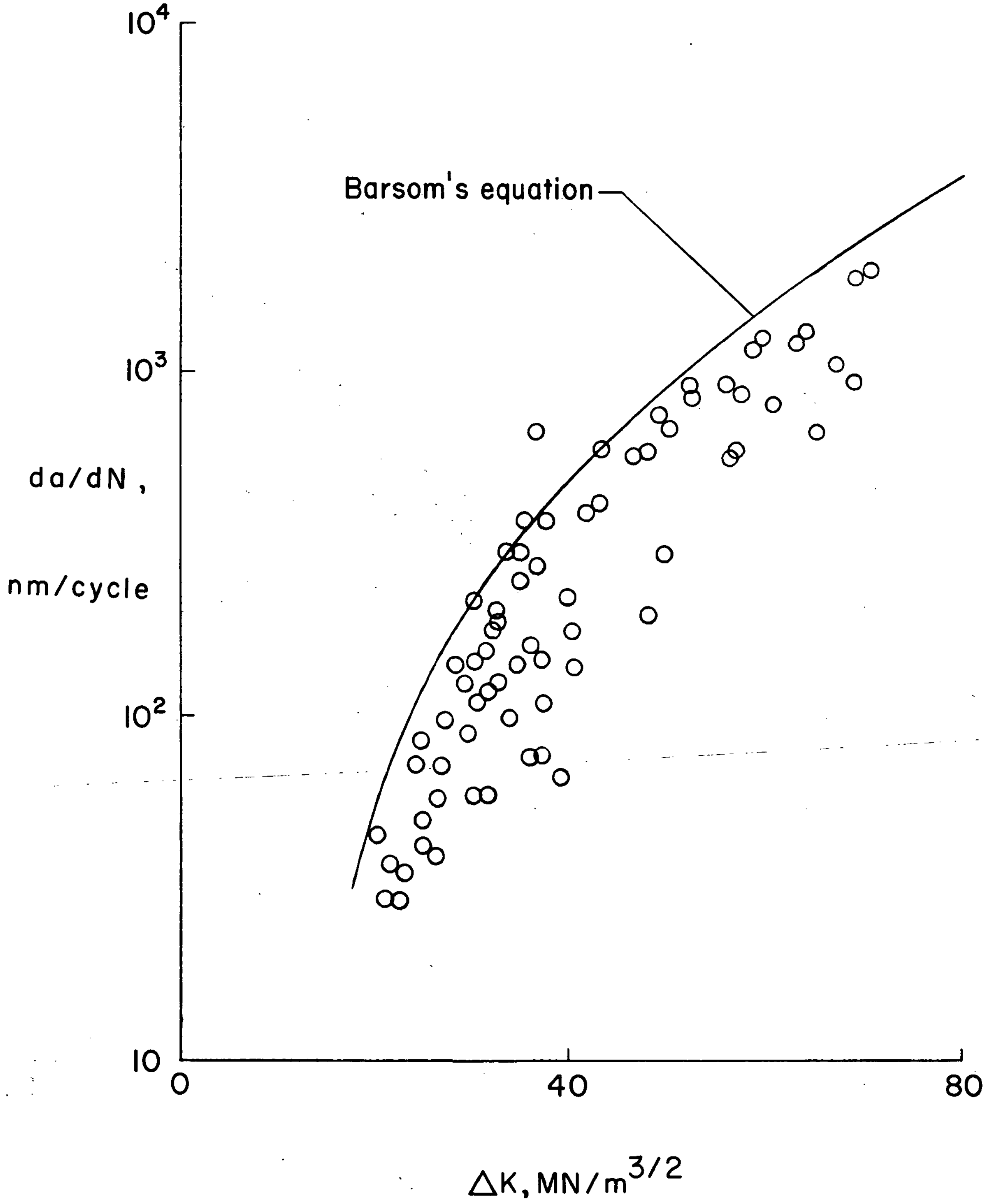

Figure 15.- Variation of da/dN with ΔK for VMS 5002. R ≈ 0.

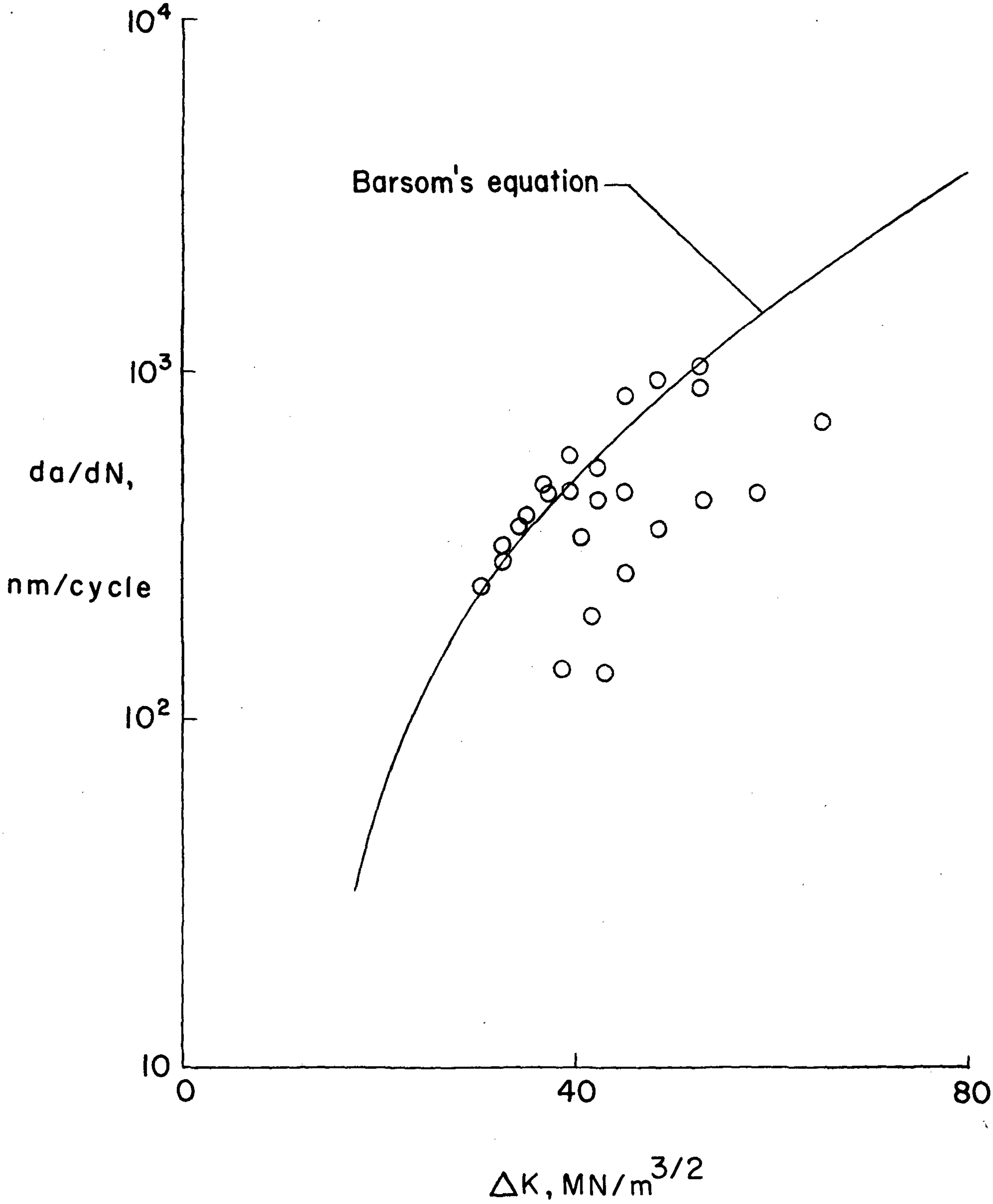

Figure 16.- Variation of da/dN with ΔK for VMS 1146A. $R \approx 0$.

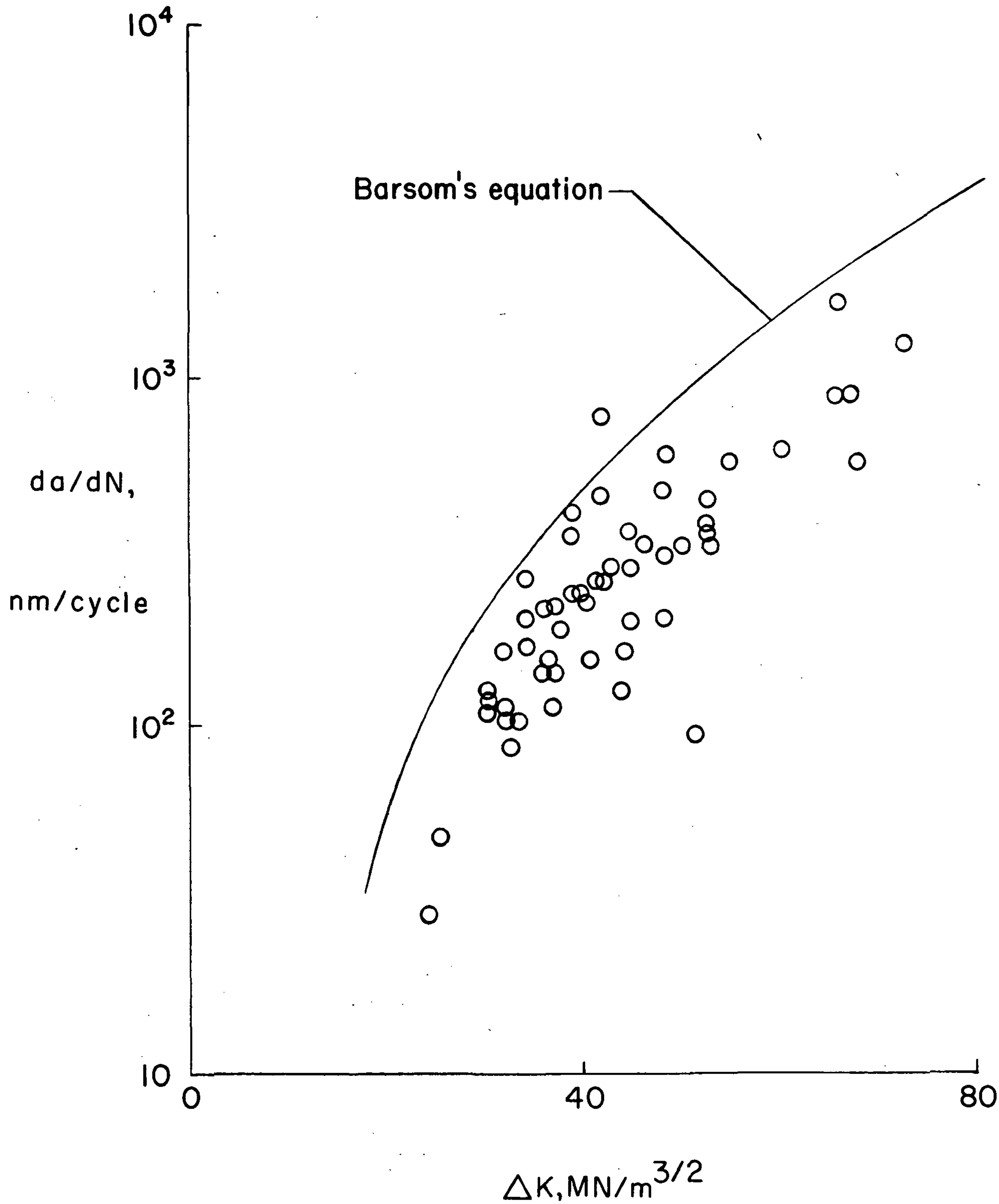

Figure 17.- Variation of da/dN with ΔK for A-225 Gr.B. $R \approx 0$.

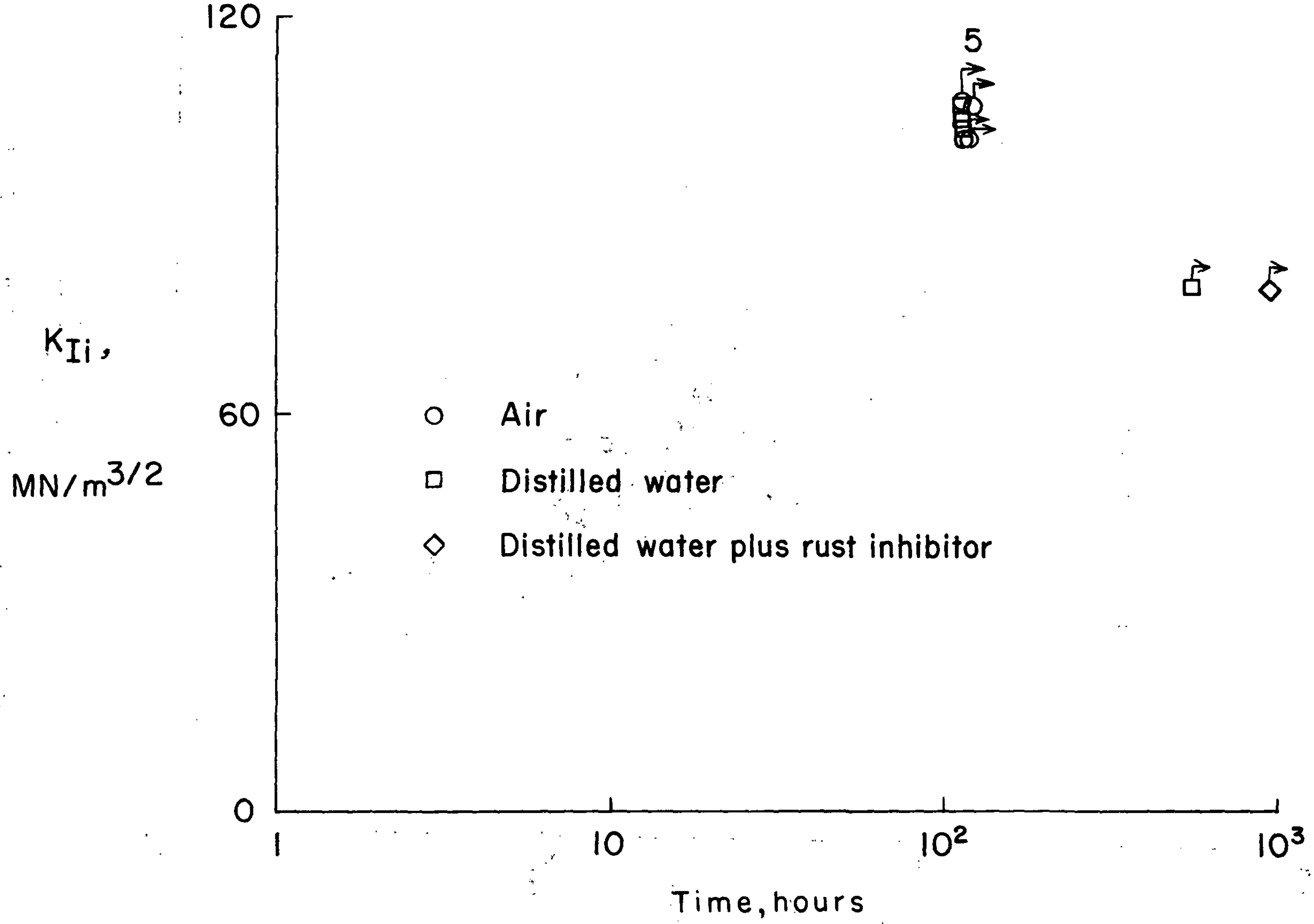

Figure 18.- Variation of K_{Ii} with test time for VMS 5002. Arrows indicate specimens which did not fail.

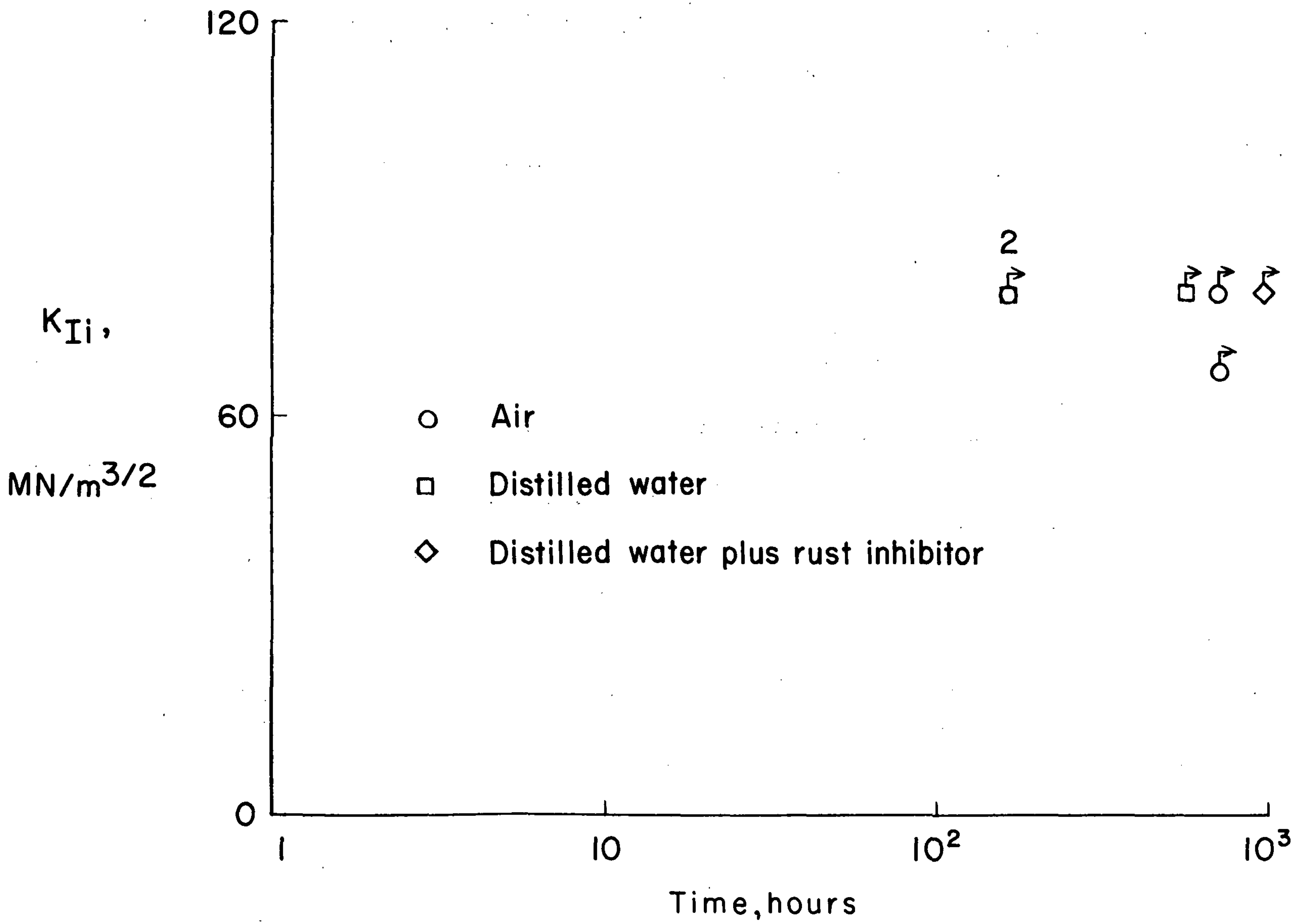

Figure 19.- Variation of K_{Ii} with test time for VMS 1146A. Arrows indicate specimens which did not fail.

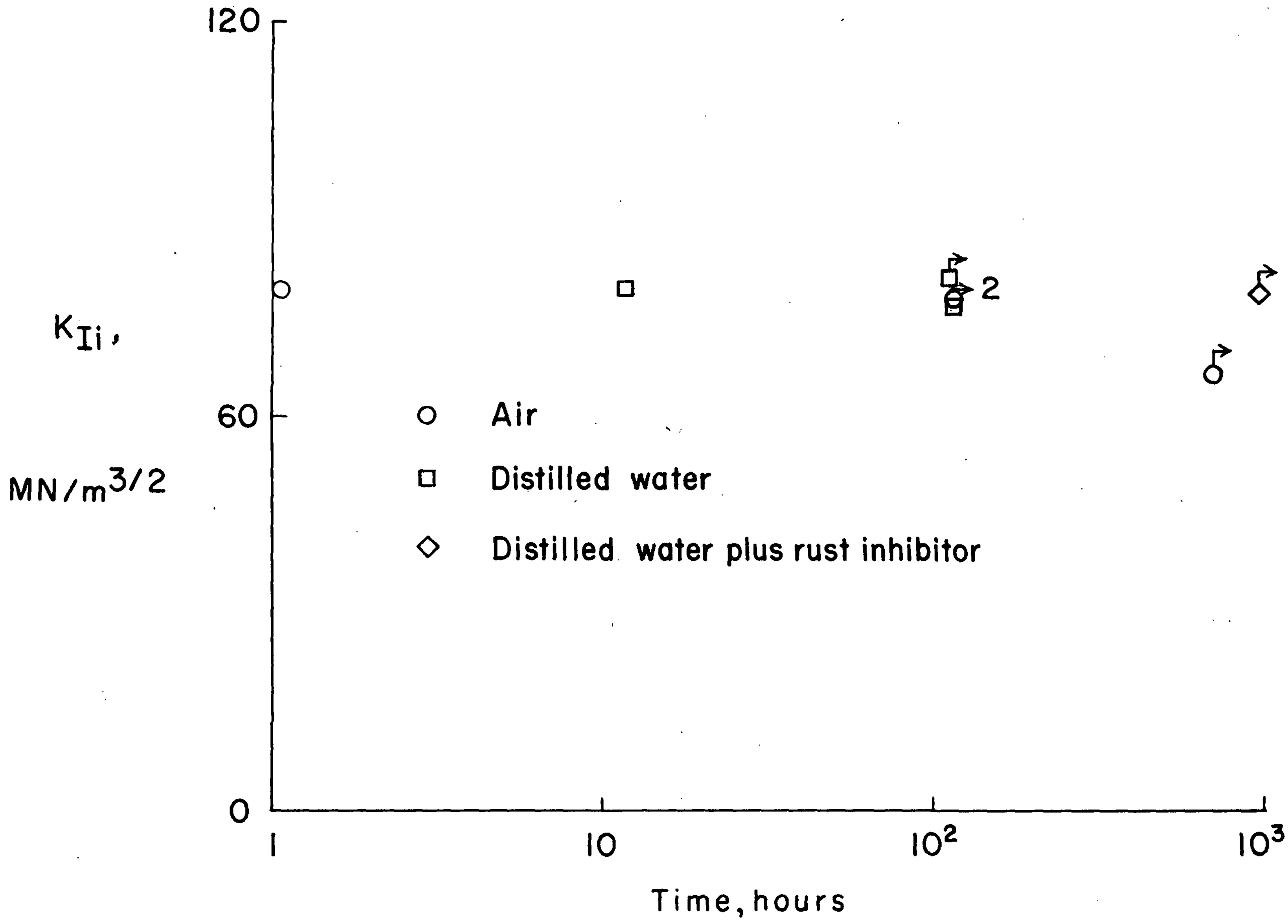

Figure 20.- Variation of K_{Ii} with test time for A-225 Gr.B. Arrows indicate specimens which did not fail.

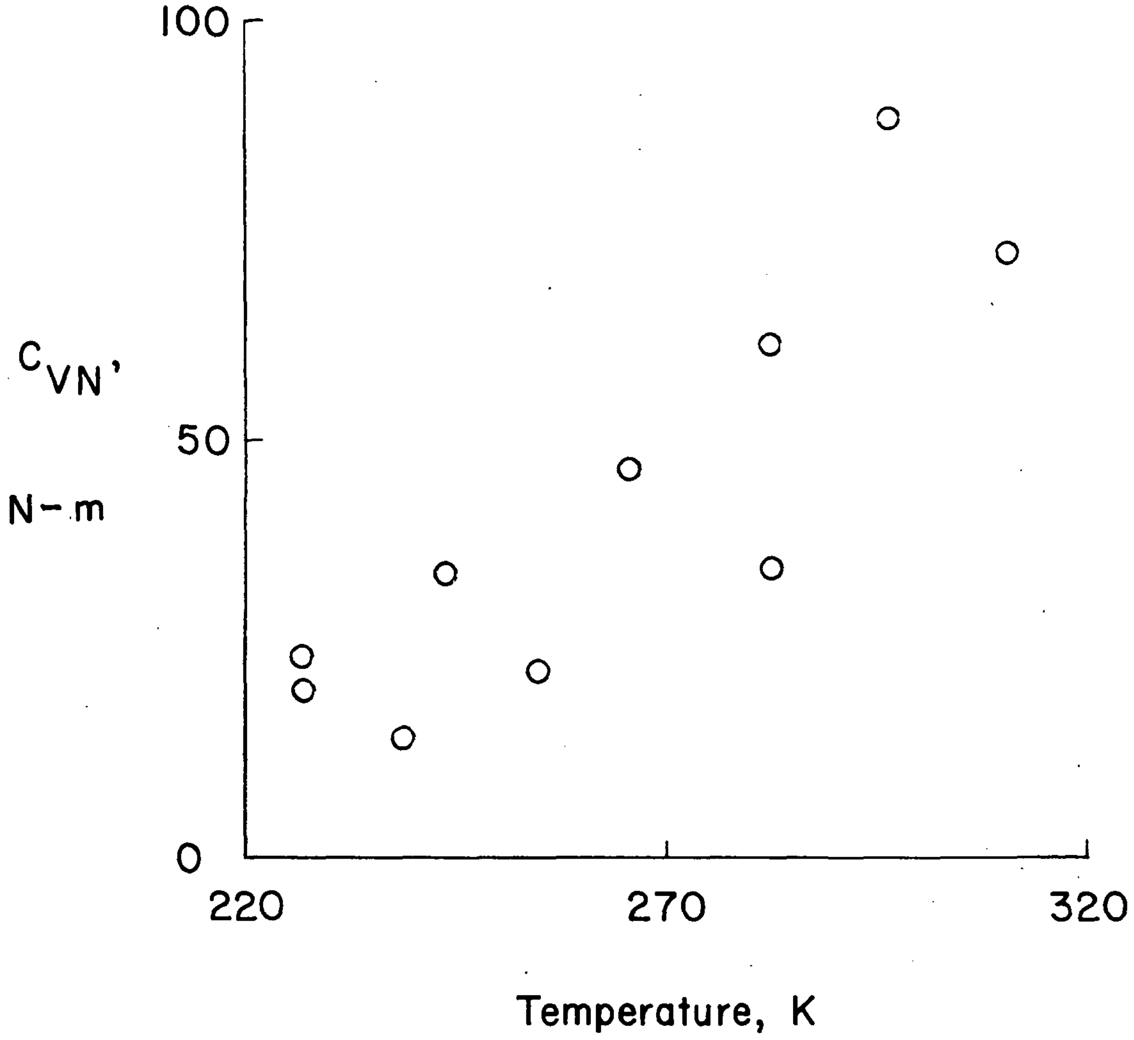

Figure 21.- Variation of C_{VN} with temperature for VMS 5002.

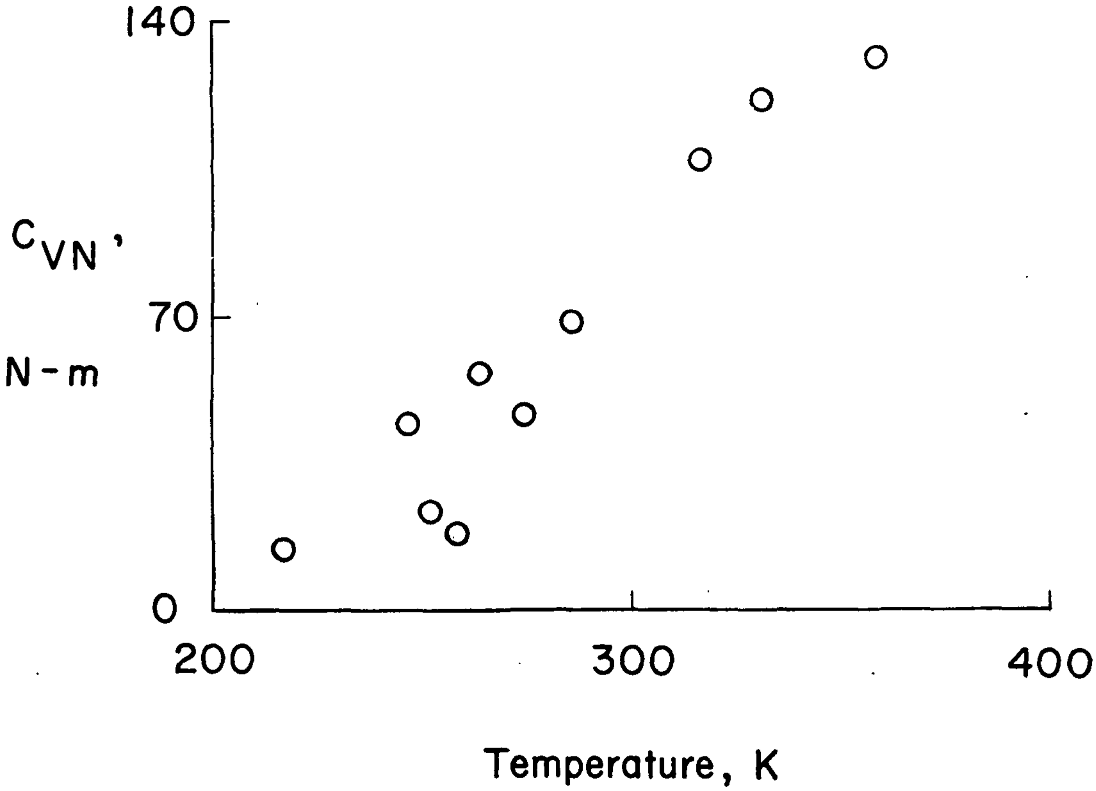

Figure 22.- Variation of C_{VN} with temperature for VMS 1146A.

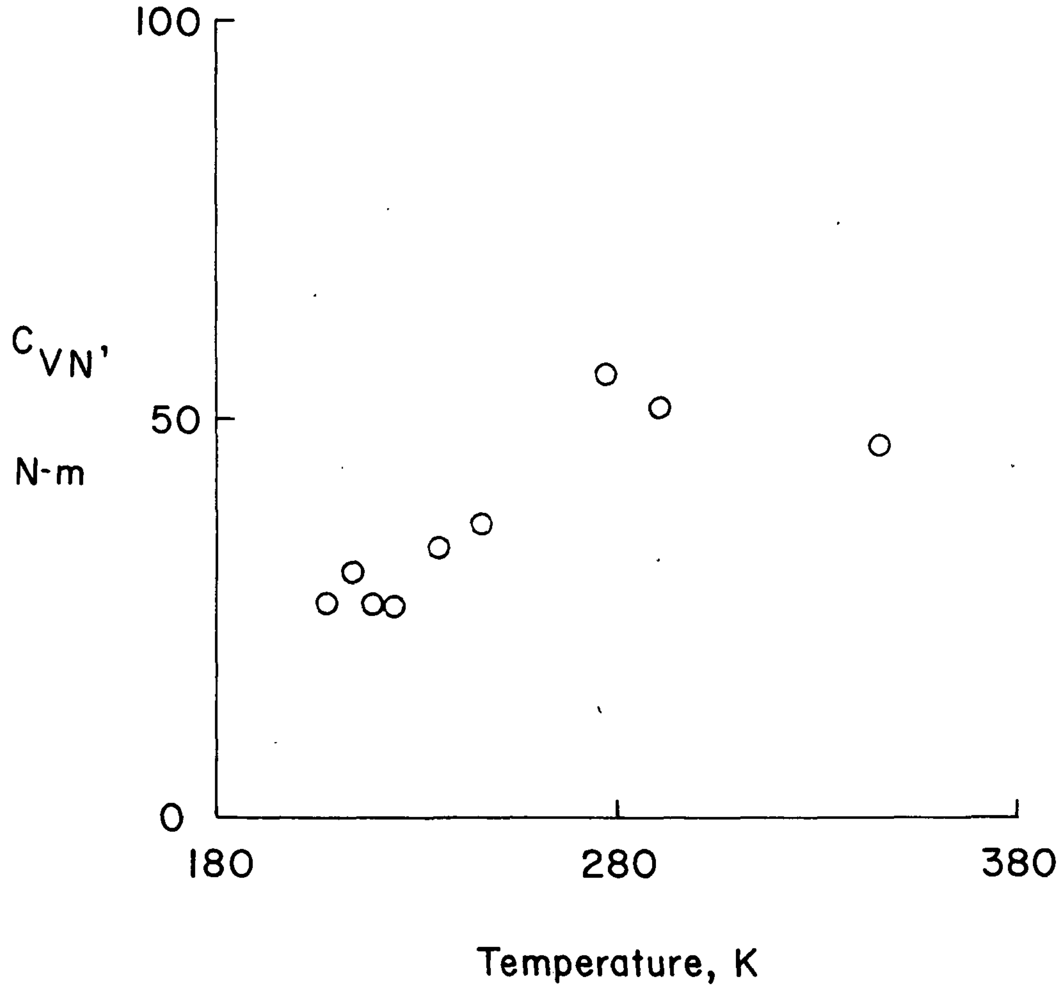

Figure 23.- Variation of C_{VN} with temperature for A-225 Gr.B.

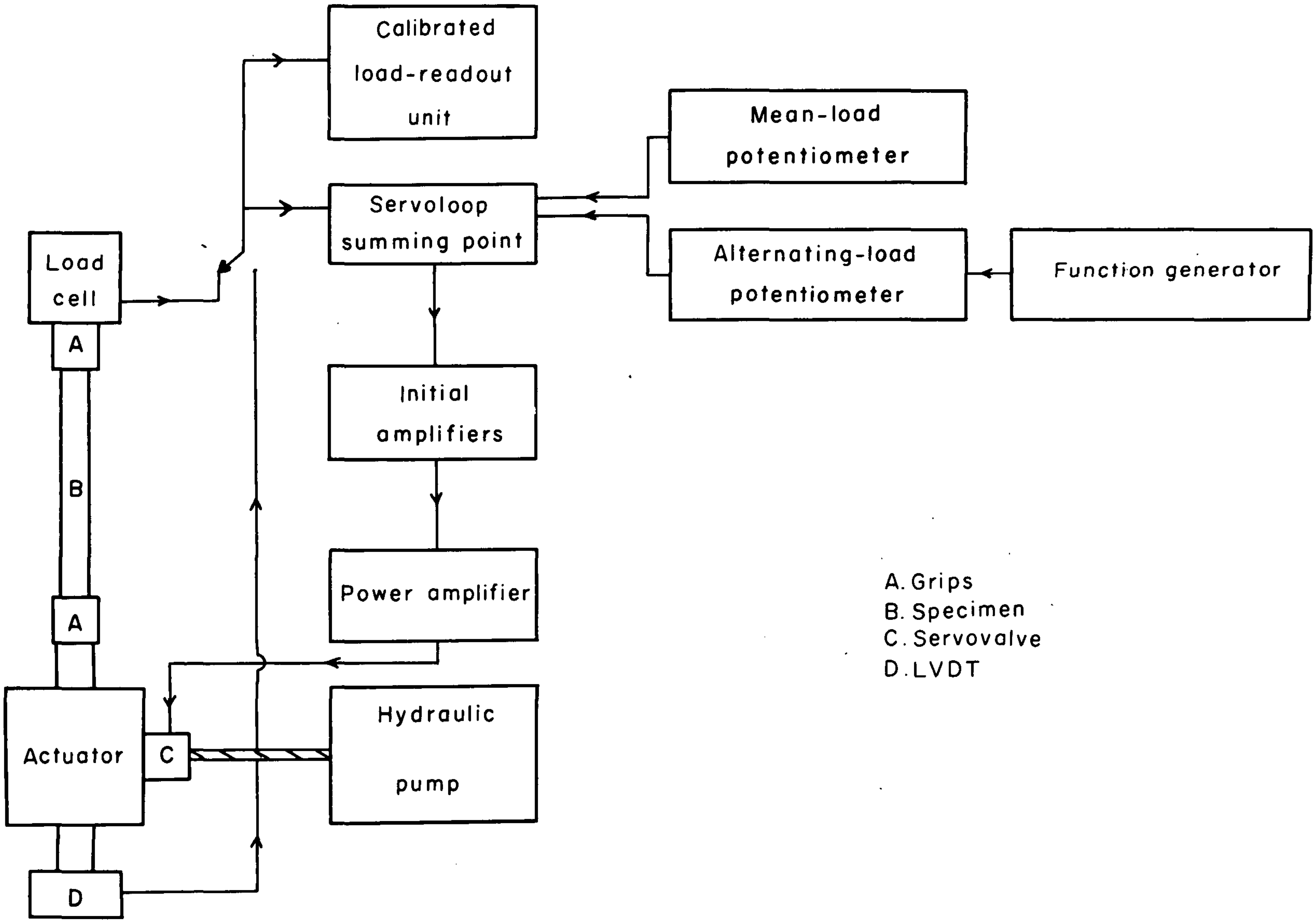

Figure 24.- Schematic diagram of loading system for 445- and 4448-kN testing machines.

NASA-Langley, 1975 L-10447

"The aeronautical and space activities of the United States shall be conducted so as to contribute . . . to the expansion of human knowledge of phenomena in the atmosphere and space. The Administration shall provide for the widest practicable and appropriate dissemination of information concerning its activities and the results thereof."

—NATIONAL AERONAUTICS AND SPACE ACT OF 1958

NASA SCIENTIFIC AND TECHNICAL PUBLICATIONS

TECHNICAL REPORTS: Scientific and technical information considered important, complete, and a lasting contribution to existing knowledge.

TECHNICAL NOTES: Information less broad in scope but nevertheless of importance as a contribution to existing knowledge.

TECHNICAL MEMORANDUMS: Information receiving limited distribution because of preliminary data, security classification, or other reasons. Also includes conference proceedings with either limited or unlimited distribution.

CONTRACTOR REPORTS: Scientific and technical information generated under a NASA contract or grant and considered an important contribution to existing knowledge.

TECHNICAL TRANSLATIONS: Information published in a foreign language considered to merit NASA distribution in English.

SPECIAL PUBLICATIONS: Information derived from or of value to NASA activities. Publications include final reports of major projects, monographs, data compilations, handbooks, sourcebooks, and special bibliographies.

TECHNOLOGY UTILIZATION PUBLICATIONS: Information on technology used by NASA that may be of particular interest in commercial and other non-aerospace applications. Publications include Tech Briefs, Technology Utilization Reports and Technology Surveys.

Details on the availability of these publications may be obtained from:

SCIENTIFIC AND TECHNICAL INFORMATION OFFICE

NATIONAL AERONAUTICS AND SPACE ADMINISTRATION

Washington, D.C. 20546